

1 **UPSCALING DIFFUSION THROUGH FIRST-ORDER**
2 **VOLUMETRIC SINKS: A HOMOGENIZATION OF BACTERIAL**
3 **NUTRIENT UPTAKE**

4 MOHIT P. DALWADI*, YANMING WANG*, JOHN R. KING†, AND NIGEL P. MINTON*

5 **Abstract.** In mathematical models that include nutrient delivery to bacteria, it is prohibitively
6 expensive to include a pointwise nutrient uptake within small bacterial regions over bioreactor length-
7 scales, and so such models often impose an effective uptake instead. In this paper, we systematically
8 investigate how the effective uptake should scale with bacterial size and other microscale properties
9 under first-order uptake kinetics. We homogenize the unsteady problem of nutrient diffusing through
10 a locally periodic array of spherical bacteria, within which it is absorbed. We introduce a general
11 model that could also be applied to other single-cell microorganisms, such as cyanobacteria, microal-
12 gae, protozoa, and yeast and we consider generalizations to arbitrary bacterial shapes, including
13 some analytic results for ellipsoidal bacteria. We explore in detail the three distinguished limits of
14 the system on the timescale of diffusion over the macroscale. When the bacterial size is of the same
15 order as the distance between them, the effective uptake has two limiting behaviours, scaling with
16 the bacterial volume for weak uptake and with the bacterial surface area for strong uptake. We
17 derive the function that smoothly transitions between these two behaviours as the system paramet-
18 ers vary. Additionally, we explore the distinguished limit in which bacteria are much smaller than
19 the distance between them and have a very strong uptake. In this limit, we find that the effective
20 uptake is bounded above as the uptake rate grows without bound; we are able to quantify this and
21 characterize the transition to the other limits we consider.

22 **Key words.** bacterial uptake, multiscale, distinguished limits, effective uptake

23 **AMS subject classifications.** 35B27, 35K57, 80A30, 92C45

24 **1. Introduction.** As the technology to manipulate the metabolic pathways of
25 microorganisms grows more sophisticated, more chemicals become industrially viable
26 targets for biosynthetic production. For example, microorganisms can be used as ‘cell
27 factories’ to produce environmentally friendly biofuels, cheaper medicines, and fine
28 chemicals [20]. In order to control and optimize the industrial production of such
29 chemicals, it is important to understand how nutrient is transported to and absorbed
30 by these microorganisms.

31 A typical experimental set-up for a cell factory involves feeding bacteria with
32 nutrient within a liquid-filled bioreactor. As bacterial movement is generally forced
33 by the fluid flow in these bioreactors, there is little relative advection close to each
34 bacterium. Thus, the nutrient absorbed by the bacteria causes a concentration gradi-
35 ent close to the bacteria that drives further nutrient towards the bacteria. While the
36 mathematical equations that govern the salient transport processes such as diffusion,
37 advection, and chemical reaction are well known [4], there is a considerable separation
38 between the longer bioreactor (0.1 – 1 m) and shorter bacterial (0.1 – 10 μm) length-
39 scales [21], which we refer to as the macroscale and microscale, respectively. Hence,
40 it is prohibitively expensive to include bacterial regions in a computational model of
41 bacterial uptake over the length of a bioreactor.

42 One method to bypass this expense is to treat the liquid and bacterial regions
43 as a single-phase domain, and to model the bacterial uptake as an effective nutrient

*Synthetic Biology Research Centre, University of Nottingham, University Park, Not-
tingham, NG7 2RD, UK (mohit.dalwadi@nottingham.ac.uk, yanming.wang@nottingham.ac.uk,
nigel.minton@nottingham.ac.uk)

†School of Mathematical Sciences, University of Nottingham, University Park, Nottingham, NG7
2RD, UK (john.king@nottingham.ac.uk)

44 sink over this domain. While this is a computationally efficient resolution, it is not
 45 immediately clear how to relate properties on the bacterial scale, such as bacterial
 46 size and kinetic uptake parameters, with this effective result. For example, one may
 47 intuitively expect the effective uptake to scale with bacterial volume for weak uptake
 48 and to scale with bacterial surface area for strong uptake. Our goal in this paper is to
 49 quantify when each of these scalings is valid, obtain the correct form of the effective
 50 uptake when neither is appropriate, and characterize the smooth transition between
 51 these canonical forms of the effective uptake as a function of the system parameters.

52 To investigate these questions, we systematically upscale the microscale problem
 53 of unsteady diffusion through and past a locally periodic array of spherical bacteria
 54 that act as volume sinks of nutrient with first-order kinetics, governed by the reaction–
 55 diffusion equation

$$56 \quad (1) \quad \frac{\partial c}{\partial t} = \nabla \cdot (\tilde{D} \nabla c) - \tilde{\lambda} c,$$

58 with continuous concentration and flux across the bacterial membrane, with set-up
 59 shown in Figure 1. Here, \tilde{D} and $\tilde{\lambda}$ are piecewise-constant functions which are discon-
 60 tinuous across each bacterial membrane, and where $\tilde{\lambda}$ vanishes outside each bacteria.
 61 Our main goal is to determine the effective uptake of the upscaled system in the
 62 distinguished limits where the effective uptake balances the macroscale diffusion, in
 63 particular when \tilde{D} and $\tilde{\lambda}$ depend on the separation distance between bacteria. To
 64 focus on the competing effects of diffusion and uptake, we do not consider advection
 65 in this problem. We show that when the effective uptake balances the macroscale
 66 diffusion over the timescale of the latter, the inclusion of just diffusion and uptake
 67 can lead to three distinguished asymptotic limits, which we comprehensively analyse.
 68 Investigating these three distinguished limits allows us to characterize the upscaled
 69 problem for general single-celled microorganisms, including cyanobacteria, microal-
 70 gae, protozoa, and yeast, for which different parameter regimes may be appropriate.
 71 To upscale this problem, we use mathematical homogenization (as outlined in, for
 72 example, [3, 28, 17]) via the method of multiple scales (also known as periodic ho-
 73 mogenization), rather than, for example, volume averaging methods [33]. We note
 74 that, in practice, both methods result in the same averaged equations [12].

75 One of the asymptotic limits we consider in this paper is a double-porosity model
 76 [1], where a coefficient (often the porosity or diffusion coefficient) varies greatly be-
 77 tween two regions and is a function of the small parameter of periodicity. A notable
 78 property of double-porosity models is that the upscaled equations often exhibit a mem-
 79 ory effect - that is, in averaging the problem from a time-local microscale problem up
 80 to a macroscale problem, the history of the problem becomes important, and this can
 81 cause a partial differential equation to be upscaled into an integro-differential equation
 82 [24], as we shall encounter in this paper. This effect is equivalent to having coupled
 83 partial differential equations to solve on the macroscale, as the equations cannot be
 84 solved one after the other, but rather must be solved simultaneously (disregarding
 85 iterative methods).

86 Another asymptotic limit we consider in this paper is that of very small bacte-
 87 ria, *i.e.* when the bacterial radius is much smaller than the distance between sphere
 88 centres. In such problems, there may be a critical size of the inner problem for which
 89 a distinguished limit arises. In [8] (see [23] for the original in French), the homog-
 90 enization of Laplace’s equation in an n -dimensional domain periodically perforated
 91 with n -dimensional spheres is considered and in the three-dimensional case the critical
 92 perforation size is identified as being proportional to the cube of the small parame-

93 ter of periodicity. In this paper, we investigate the distinguished limit in which the
94 bacterial size has the same critical scaling as these cases, combined with a very large
95 uptake coefficient. In contrast to the perforated domain cases mentioned above, in
96 this paper we must also solve a problem within each bacterium. We homogenize
97 this case in a similar manner to [6], where the authors use the method of matched
98 asymptotic expansions within a homogenization procedure to calculate an effective
99 boundary condition for the shielding of a Faraday cage.

100 There has been previous work homogenizing solute transport problems with ad-
101 sorption or chemical reaction within disconnected periodic subdomains of the full
102 domain, and we next discuss several notable examples of particular relevance to this
103 paper. In [18], the authors consider Stokes flow coupled with an advection–diffusion
104 solute transport problem past a periodic array of permeable obstacles. The solute can
105 diffuse within the obstacle, and there are general nonlinear reaction terms in both the
106 fluid and obstacle phases. The solute concentrations in these phases are coupled via
107 continuity of mass flux and one of six different additional conditions. The diffusion
108 coefficient within the obstacle phase is much smaller than the diffusion coefficient
109 within the fluid phase, yielding a double-porosity model that results in a memory
110 term in the homogenized equation. In [9], the authors consider steady diffusion with
111 local forcing past a periodic array of obstacles for two cases; the second of these is rel-
112 evant for our work, and involves diffusion and nonlinear uptake within the obstacles,
113 coupled via continuity of concentration and concentration flux on the surface of the
114 obstacles. The diffusion coefficients inside and outside the obstacles are of the same
115 order. In [29], Navier–Stokes flow in capillaries is coupled to Darcy flow in tissue, and
116 these both feed into an advection–diffusion equation for drug transport through both
117 phases, with a linear uptake term within the tissue, all in a periodic domain. The
118 flow equations are upscaled in the double-porosity limit, and the drug transport equa-
119 tions are upscaled for several different coupling conditions, with a focus on advective
120 transport. In [15], the authors consider diffusive transport with nonlinear reaction
121 terms in a periodic domain containing a multiply connected subdomain with different
122 diffusion coefficient and reaction terms from the rest of the domain. At the interface
123 between these regions, the fluxes are general nonlinear functions of the concentrations
124 on either side of the interface.

125 In each of the papers discussed in the above paragraph, the structure of the peri-
126 odic microscale is fairly general, allowing for homogenized equations to be calculated
127 in terms of general cell problems. While this generality is valuable, it also means that
128 effective terms are not calculated explicitly. Thus, the generality of these problems is
129 not conducive to a systematic investigation of how the effective parameters vary as a
130 function of the system parameters.

131 We mainly consider spherical bacteria (*cocci*), whose radius can vary slowly over
132 the macroscale, but also consider the generalization to arbitrary bacterial shapes in
133 the Appendix, including some analytic results for ellipsoidal bacteria. Traditional ho-
134 mogenization techniques require a strictly periodic microscale geometry, but there are
135 methods to extend these techniques to problems with a microscale that varies over the
136 macroscale [31, 27, 5]. These extensions have formal roots in [2] and [7], and there has
137 been a significant amount of recent applied work into homogenizing specific problems
138 involving reaction and diffusion processes, such as [14, 26]. The key idea behind ex-
139 tending standard homogenization theory from a strictly periodic microstructure to a
140 locally periodic microstructure is to use a level-set function in both the microscale and
141 macroscale variables to define the microstructure [32]. Consequently, this extension
142 is sometimes referred to as the level-set framework. In general, this method requires

143 a different cell problem to be solved at every point in the macroscale rather than
 144 just once for the entire problem (as is the case for standard homogenization theory),
 145 but this additional computational expense can be bypassed by imposing a specific
 146 one-parameter shape on the microstructure [5, 10]. This is the route we take in the
 147 main text of this paper; restricting our main analysis to spherical bacteria allows us to
 148 maximize our analytic progress and, consequently, to systematically analyse the form
 149 of the effective uptake in the three distinguished limits we consider, yielding greater
 150 physical insight into the system behaviour as a function of the system parameters.
 151 Additionally, and to the same end, we neglect any internal structure of the bacteria,
 152 treating the bacterial interior as homogeneous. Finally, we note that, in this paper,
 153 we only use ‘cell’ in the language of mathematical homogenization and never in the
 154 biological sense; that is, we only use ‘cell’ to refer to the periodic unit cell domain in
 155 what is commonly referred to as a ‘cell problem’ in mathematical homogenization.

156 The structure of this paper is as follows. We present a dimensional description of
 157 the bacterial uptake model in §2, and form the dimensionless problem. We then formu-
 158 late the problem to be upscaled via homogenization theory in §3, and upscale this
 159 problem for three distinguished limits in §3.1, §3.2, and §3.3. We briefly consider the
 160 generalization of these results to arbitrary bacterial shapes in Appendix A, including
 161 some analytic results for ellipsoidal bacteria in one sub-limit. Finally, we discuss the
 162 physical implications of these results and conclude in §4.

163 **2. Model description.** We consider the diffusion and uptake of nutrient through
 164 a colony of bacteria within a passive medium, which could model fluid within a biore-
 165 actor or the extracellular polymeric substance within a biofilm. We describe the
 166 nutrient distribution in terms of its concentration, which is defined in the medium
 167 and bacterial phases as $\tilde{c}(\tilde{\mathbf{x}}, \tilde{t})$ and $\tilde{C}(\tilde{\mathbf{x}}, \tilde{t})$, respectively. Here, \tilde{c} and \tilde{C} are given in
 168 terms of the molarity of the concentration, $\tilde{\mathbf{x}}$ is the spatial vector coordinate, and
 169 \tilde{t} is time. We assume that the nutrient diffuses through the passive medium with
 170 constant diffusion coefficient D_m , and through the bacteria with constant diffusion
 171 coefficient D_b . Additionally, we assume that the nutrient uptake occurs only within
 172 the bacteria, and that the uptake is proportional to the nutrient concentration with
 173 rate of proportionality λ .

174 We model the bacteria as a collection of spheres whose centres are located on a
 175 cubic lattice at a distance ϵl apart, where ϵ is a small dimensionless parameter and l
 176 is the typical length of the entire domain. The radii of the bacteria can vary slowly in
 177 space, and a bacterium centred at $\tilde{\mathbf{x}}$ has radius $\tilde{R}(\tilde{\mathbf{x}})$. For simplicity, we retain a fixed
 178 cell size. We only consider non-overlapping spheres, and thus $2\tilde{R} < \epsilon l$. The bacterial
 179 and medium phases are denoted as $\Omega_b \subset \mathbb{R}^3$ and $\Omega_m \subset \mathbb{R}^3$, respectively. We denote
 180 the entire spatial domain as $\Omega = \Omega_b \cup \Omega_m \subset \mathbb{R}^3$, and note that $\Omega_b \cap \Omega_m = \emptyset$. Finally,
 181 we also denote the boundary between the two phases as $\partial\Omega_b$, which we refer to as the
 182 ‘bacterial membrane’, or just ‘membrane’. To couple the concentrations across the
 183 bacterial membrane, we assume continuity of concentration and concentration flux.

184 Mathematically, we have the dimensional problem

$$185 \quad (2a) \quad \frac{\partial \tilde{c}}{\partial \tilde{t}} = D_m \nabla^2 \tilde{c} \quad \text{for } \tilde{\mathbf{x}} \in \Omega_m,$$

$$186 \quad (2b) \quad \frac{\partial \tilde{C}}{\partial \tilde{t}} = D_b \nabla^2 \tilde{C} - \lambda \tilde{C} \quad \text{for } \tilde{\mathbf{x}} \in \Omega_b,$$

$$187 \quad (2c) \quad \tilde{c} = \tilde{C} \quad \text{for } \tilde{\mathbf{x}} \in \partial\Omega_b,$$

$$188 \quad (2d) \quad \mathbf{n} \cdot D_m \nabla \tilde{c} = \mathbf{n} \cdot D_b \nabla \tilde{C} \quad \text{for } \tilde{\mathbf{x}} \in \partial\Omega_b,$$

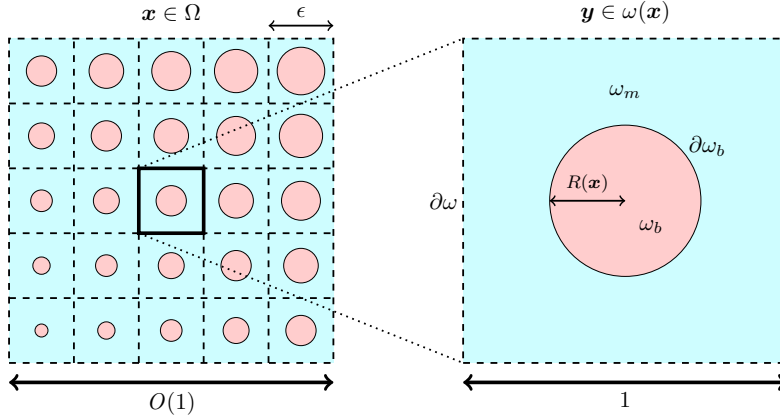


FIG. 1. A two-dimensional projection of the three-dimensional problem we consider. The full problem is shown in the left figure, from which the cell problem (with $\mathbf{y} \in [-1/2, 1/2]^3$) is magnified and shown in the right figure. The nutrient diffuses with different diffusion coefficients in the blue passive medium and in the pink bacteria, and is absorbed within the bacteria at a rate proportional to its concentration. We couple the regions via continuity of concentration and concentration flux.

$$189 \quad (2e) \quad \tilde{c}(\tilde{\mathbf{x}}, 0) = \tilde{c}_{\text{init}}(\tilde{\mathbf{x}}) \quad \text{for } \tilde{\mathbf{x}} \in \Omega_m,$$

$$190 \quad (2f) \quad \tilde{C}(\tilde{\mathbf{x}}, 0) = \tilde{c}_{\text{init}}(\tilde{\mathbf{x}}) \quad \text{for } \tilde{\mathbf{x}} \in \Omega_b.$$

192 where \mathbf{n} is the unit normal of the bacterial membrane pointing into the surrounding
 193 medium. The function $\tilde{c}_{\text{init}}(\tilde{\mathbf{x}})$ appearing in the initial conditions (2e) and (2f) is con-
 194 tinuous across the bacterial membrane and allows for a slow variation of the nutrient
 195 concentration in space. To close the system (2), we also require boundary conditions
 196 at the external boundary of Ω . However, to keep the generality of our analysis we
 197 will not impose a specific form in this paper.

198 In general, the typical diameter of bacterial *cocci* is around $2\tilde{R} \approx 1 \mu\text{m}$, and a fer-
 199 mentation process would start with a cell density of around 10^8 cells/ml and end with
 200 a cell density of around 10^{11} cells/ml, corresponding to the approximate cell spacing
 201 $\epsilon l \approx 2 - 20 \mu\text{m}$ [21, 22]. Additionally, cell growth occurs on a much slower timescale
 202 than nutrient transport. It is generally possible to obtain the diffusion coefficient of
 203 a given nutrient within water and, for example, the diffusivities of dissolved carbon
 204 dioxide, nitrogen, and oxygen within water at room temperature are each around
 205 $2 \text{cm}^2/\text{s}$ (with a maximum variation away from this value of 6%). However, it is much
 206 trickier to get pointwise diffusion and uptake coefficients within bacteria due to the
 207 difficulties in isolating and imaging a single bacterium. Partly for this reason, and also
 208 for a more general analysis (protozoa, for example, can have diameters $> 100 \mu\text{m}$),
 209 it will be instructive to consider the various distinguished asymptotic limits of this
 210 problem.

211 **2.1. Dimensionless equations.** We scale the variables via $\tilde{\mathbf{x}} = l\mathbf{x}$, $\tilde{t} = (l^2/D_m)t$,
 212 $\tilde{R} = \epsilon l R$, $(\tilde{c}, \tilde{C}, \tilde{c}_{\text{init}}) = c_\infty(c, C, c_{\text{init}})$, where c_∞ is a characteristic concentration scale,
 213 to yield the dimensionless equations

$$214 \quad (3a) \quad \frac{\partial c}{\partial t} = \nabla^2 c \quad \text{for } \mathbf{x} \in \Omega_m,$$

$$215 \quad (3b) \quad \frac{\partial C}{\partial t} = D(\nabla^2 C - \mu C) \quad \text{for } \mathbf{x} \in \Omega_b,$$

$$216 \quad (3c) \quad c = C \quad \text{for } \mathbf{x} \in \partial\Omega_b,$$

$$217 \quad (3d) \quad \mathbf{n} \cdot \nabla c = \mathbf{n} \cdot D\nabla C \quad \text{for } \mathbf{x} \in \partial\Omega_b,$$

$$218 \quad (3e) \quad c(\mathbf{x}, 0) = c_{\text{init}}(\mathbf{x}) \quad \text{for } \mathbf{x} \in \Omega_m,$$

$$219 \quad (3f) \quad C(\mathbf{x}, 0) = c_{\text{init}}(\mathbf{x}) \quad \text{for } \mathbf{x} \in \Omega_b.$$

221 where $D = D_b/D_m$ is the ratio of diffusion coefficient in the medium to that in the
 222 bacteria, and $\mu = \lambda^2/D_b$ is the ratio of the timescales of diffusion within the bacteria
 223 to uptake. The inclusion of the dimensionless diffusivity D in the definition of the
 224 dimensionless uptake rate $D\mu$ is for subsequent convenience. We do not specify the
 225 asymptotic orders of these dimensionless parameters yet, but later we consider the
 226 three asymptotic limits over the timescale of macroscale diffusion in the medium,
 227 where $t = O(1)$.

228 In dimensionless units, the bacteria now form a cubic lattice of spheres whose
 229 centres are a distance of ϵ apart, and a bacterium centred at \mathbf{x} has radius $\epsilon R(\mathbf{x})$. A
 230 schematic of this set-up is shown in figure 1.

231 **3. Deriving effective equations.** Our goal is to upscale the governing equa-
 232 tions (3) using a homogenization procedure via the method of multiple scales. Essen-
 233 tially, we introduce the additional spatial variable

$$234 \quad (4) \quad \mathbf{y} = \frac{\mathbf{x} - \lfloor \mathbf{x} \rfloor}{\epsilon} - \mathbf{b},$$

235 where we treat \mathbf{x} and \mathbf{y} as independent. In (4), we introduce the constant translation
 236 vector $\mathbf{b} = (1/2, 1/2, 1/2)$ for notational purposes. Thus, the microscale variable
 237 $\mathbf{y} \in [-1/2, 1/2]^3$ is defined within a unit cell $\omega(\mathbf{x})$, centred around one bacterium,
 238 and our dependent variables are now $c(\mathbf{x}, \mathbf{y}, t)$ and $C(\mathbf{x}, \mathbf{y}, t)$. The extra freedom that
 239 arises from introducing \mathbf{y} is later removed by imposing that the problem is 1-periodic
 240 in each component of \mathbf{y} . Within each cell, we define several regions for convenience.
 241 The bacterium and medium phases are defined as $\omega_b(\mathbf{x})$ and $\omega_m(\mathbf{x})$, respectively. The
 242 spherical bacterial membrane between these two phases is defined as $\partial\omega_b(\mathbf{x})$. Finally,
 243 the cubic outer boundary of the cell is defined as $\partial\omega$. Formally, these sets are defined
 244 as

$$246 \quad (5a) \quad \omega_b = \{\mathbf{y} \in [-1/2, 1/2]^3 : \|\mathbf{y}\| < R(\mathbf{x})\},$$

$$247 \quad (5b) \quad \omega_m = \{\mathbf{y} \in [-1/2, 1/2]^3 : \|\mathbf{y}\| > R(\mathbf{x})\},$$

$$248 \quad (5c) \quad \partial\omega_b = \{\mathbf{y} \in [-1/2, 1/2]^3 : \|\mathbf{y}\| = R(\mathbf{x})\},$$

$$249 \quad (5d) \quad \partial\omega = \{\mathbf{y} \in [-1/2, 1/2]^3 : \|\mathbf{y}\|_\infty = 1/2\},$$

251 where $\|\cdot\|$ and $\|\cdot\|_\infty$ are the three-dimensional Euclidean and infinity norms, respec-
 252 tively.

253 We are interested in deriving effective governing equations for two quantities.
 254 Firstly, $\widehat{c}(\mathbf{x}, t)$, the intrinsic-averaged concentration within the medium, defined as

$$255 \quad (6a) \quad \widehat{c}(\mathbf{x}, t) = \frac{1}{|\omega_m(\mathbf{x})|} \int_{\omega_m(\mathbf{x})} c(\mathbf{x}, \mathbf{y}, t) \, d\mathbf{y},$$

257 where $|\cdot|$ is the volume. The intrinsic-averaged concentration is important because
 258 it is the experimentally measurable concentration. Secondly, $\bar{c}(\mathbf{x}, t)$, the volumetric-
 259 averaged concentration, defined as

$$260 \quad \bar{c}(\mathbf{x}, t) = \frac{1}{|\omega(\mathbf{x})|} \left(\int_{\omega_m(\mathbf{x})} c(\mathbf{x}, \mathbf{y}, t) \, d\mathbf{y} + \int_{\omega_b(\mathbf{x})} C(\mathbf{x}, \mathbf{y}, t) \, d\mathbf{y} \right)$$

$$(6b) \quad = \int_{\omega_m(\mathbf{x})} c(\mathbf{x}, \mathbf{y}, t) d\mathbf{y} + \int_{\omega_b(\mathbf{x})} C(\mathbf{x}, \mathbf{y}, t) d\mathbf{y}.$$

The volumetric-averaged concentration is a fundamental physical quantity of interest, as it can be used to determine the the total number of moles of nutrient in the system.

Treating each dependent variable as a function of both \mathbf{x} and \mathbf{y} , the spatial derivatives transform as follows

$$(7) \quad \nabla \mapsto \nabla_{\mathbf{x}} + \frac{1}{\epsilon} \nabla_{\mathbf{y}},$$

where $\nabla_{\mathbf{x}}$ and $\nabla_{\mathbf{y}}$ refer to the nabla operator in the \mathbf{x} - and \mathbf{y} -coordinate systems respectively. The spatial transformation (7) also causes the unit normal on the boundary to transform (as also occurs in, for example, [31, 5]). This can be seen by defining the function $\chi(\mathbf{x}, \mathbf{y}) = \|\mathbf{y}\| - R(\mathbf{x})$, noting that the bacterial membrane is defined by $\chi = 0$ and thus $\mathbf{n} = \nabla\chi/\|\nabla\chi\|$, then using (7) to yield

$$(8) \quad \mathbf{n} \mapsto \frac{\mathbf{n}_{\mathbf{y}} - \epsilon \nabla_{\mathbf{x}} R}{\|\mathbf{n}_{\mathbf{y}} - \epsilon \nabla_{\mathbf{x}} R\|},$$

where $\mathbf{n}_{\mathbf{y}} = \mathbf{y}/\|\mathbf{y}\|$. This transformation of the boundary is sometimes referred to as the level-set framework, as discussed in §1.

Using the transformations (7) and (8), the dimensionless governing equations (3) become

$$(9a) \quad \epsilon^2 \frac{\partial c}{\partial t} = (\nabla_{\mathbf{y}} + \epsilon \nabla_{\mathbf{x}}) \cdot (\nabla_{\mathbf{y}} + \epsilon \nabla_{\mathbf{x}}) c \quad \text{for } \mathbf{y} \in \omega_m(\mathbf{x}),$$

$$(9b) \quad \epsilon^2 \frac{\partial C}{\partial t} = D (\nabla_{\mathbf{y}} + \epsilon \nabla_{\mathbf{x}}) \cdot (\nabla_{\mathbf{y}} + \epsilon \nabla_{\mathbf{x}}) C - \epsilon^2 D \mu C \quad \text{for } \mathbf{y} \in \omega_b(\mathbf{x}),$$

$$(9c) \quad c = C \quad \text{for } \mathbf{y} \in \partial\omega_b(\mathbf{x}),$$

$$(9d) \quad (\mathbf{n}_{\mathbf{y}} - \epsilon \nabla_{\mathbf{x}} R) \cdot (\nabla_{\mathbf{y}} + \epsilon \nabla_{\mathbf{x}}) c = (\mathbf{n}_{\mathbf{y}} - \epsilon \nabla_{\mathbf{x}} R) \cdot D (\nabla_{\mathbf{y}} + \epsilon \nabla_{\mathbf{x}}) C \quad \text{for } \mathbf{y} \in \partial\omega_b(\mathbf{x}),$$

$$(9e) \quad c(\mathbf{x}, \mathbf{y}, 0) = c_{\text{init}}(\mathbf{x}) \quad \text{for } \mathbf{y} \in \omega_m(\mathbf{x}),$$

$$(9f) \quad C(\mathbf{x}, \mathbf{y}, 0) = c_{\text{init}}(\mathbf{x}) \quad \text{for } \mathbf{y} \in \omega_b(\mathbf{x}),$$

$$(9g) \quad c \text{ periodic} \quad \text{for } \mathbf{y} \in \partial\omega.$$

where (9g) is imposed to remove secular terms in the method of multiple scales. Here and hereafter, any condition similar to (9g) refers only to periodicity in the dependent variable \mathbf{y} .

We are interested in the physical scenarios in which the effective uptake balances the macroscale diffusion over the timescale of the latter, which occurs over $t = O(1)$. There are three distinguished asymptotic limits: (i) standard diffusion, uptake, and obstacle size; (ii) small diffusion, large uptake, and standard obstacle size; (iii) standard diffusion, very large uptake, and small obstacle size. We summarize the three asymptotic limits in Table 1. We note that, in the absence of any source or sink terms from the external boundary, the removal rate of nutrient in the system can be deduced from (3), as follows

$$(10) \quad \frac{\partial}{\partial t} \left(\int_{\Omega_m} c d\mathbf{x} + \int_{\Omega_b} C d\mathbf{x} \right) = -\mu D \int_{\Omega_b} C d\mathbf{x}.$$

When uptake within a bacterium occurs over the entire bacterium domain and not just within a boundary layer near the bacterial membrane, we see from (10) that an

TABLE 1

A summary of the three distinguished asymptotic limits we consider in this paper. Note that R has already been scaled by ϵ so that, when $O(1)$, it is of the same asymptotic order as the periodic-cell size.

| | D | μ | R |
|--------|-----------------|-------------------|-----------------|
| Case 1 | $O(1)$ | $O(1)$ | $O(1)$ |
| Case 2 | $O(\epsilon^2)$ | $O(1/\epsilon^2)$ | $O(1)$ |
| Case 3 | $O(1)$ | $O(1/\epsilon^6)$ | $O(\epsilon^2)$ |

$O(1)$ uptake timescale (corresponding to diffusion over the timescale of macroscale diffusion) occurs when $\mu DR^3 = O(1)$. This constraint helps to elucidate the relative scalings within each case in Table 1. We proceed by homogenizing the system in each of the three cases mentioned above.

3.1. Case 1 - standard diffusion, uptake, and obstacle size: $D = O(1)$, $\mu = O(1)$, $R = O(1)$. The first distinguished limit we consider is $D = O(1)$, $\mu = O(1)$, and $R = O(1)$. While this limit is only a specific example of the general classical case (§5.3 in [16]) with a discontinuous diffusion coefficient, it does provide the distinguished limit for the effective diffusion for the remaining cases and so we include it for completeness. To upscale the system, we introduce the asymptotic expansions

$$(11a) \quad c = c_0(\mathbf{x}, \mathbf{y}, t) + \epsilon c_1(\mathbf{x}, \mathbf{y}, t) + \epsilon^2 c_2(\mathbf{x}, \mathbf{y}, t) + O(\epsilon^3),$$

$$(11b) \quad C = C_0(\mathbf{x}, \mathbf{y}, t) + \epsilon C_1(\mathbf{x}, \mathbf{y}, t) + \epsilon^2 C_2(\mathbf{x}, \mathbf{y}, t) + O(\epsilon^3),$$

substitute these into (9), and equate terms of equal magnitude.

The leading-order terms in (9) are

$$(12a) \quad 0 = \nabla_{\mathbf{y}}^2 c_0 \quad \text{for } \mathbf{y} \in \omega_m(\mathbf{x}),$$

$$(12b) \quad 0 = D \nabla_{\mathbf{y}}^2 C_0 \quad \text{for } \mathbf{y} \in \omega_b(\mathbf{x}),$$

$$(12c) \quad c_0 = C_0 \quad \text{for } \mathbf{y} \in \partial\omega_b(\mathbf{x}),$$

$$(12d) \quad \mathbf{n}_{\mathbf{y}} \cdot \nabla_{\mathbf{y}} c_0 = D \mathbf{n}_{\mathbf{y}} \cdot \nabla_{\mathbf{y}} C_0 \quad \text{for } \mathbf{y} \in \partial\omega_b(\mathbf{x}),$$

$$(12e) \quad c_0(\mathbf{x}, \mathbf{y}, 0) = c_{\text{init}}(\mathbf{x}) \quad \text{for } \mathbf{y} \in \omega_m(\mathbf{x}),$$

$$(12f) \quad C_0(\mathbf{x}, \mathbf{y}, 0) = c_{\text{init}}(\mathbf{x}) \quad \text{for } \mathbf{y} \in \omega_b(\mathbf{x}),$$

$$(12g) \quad c_0 \text{ periodic} \quad \text{for } \mathbf{y} \in \partial\omega.$$

The system (12) yields solutions that are independent of \mathbf{y} , thus $c_0 = c_0(\mathbf{x}, t)$ and $C_0 = C_0(\mathbf{x}, t)$, with $c_0 = C_0$ and $c_0(\mathbf{x}, 0) = C_0(\mathbf{x}, 0) = c_{\text{init}}(\mathbf{x})$. To close the problem at leading order, we must derive a solvability condition from higher asymptotic orders.

The relevant $O(\epsilon)$ terms in (9) yield

$$(13a) \quad 0 = \nabla_{\mathbf{y}}^2 c_1 \quad \text{for } \mathbf{y} \in \omega_m(\mathbf{x}),$$

$$(13b) \quad 0 = D \nabla_{\mathbf{y}}^2 C_1 \quad \text{for } \mathbf{y} \in \omega_b(\mathbf{x}),$$

$$(13c) \quad c_1 = C_1 \quad \text{for } \mathbf{y} \in \partial\omega_b(\mathbf{x}),$$

$$(13d) \quad \mathbf{n}_{\mathbf{y}} \cdot (\nabla_{\mathbf{y}} c_1 + \nabla_{\mathbf{x}} c_0) = D \mathbf{n}_{\mathbf{y}} \cdot (\nabla_{\mathbf{y}} C_1 + \nabla_{\mathbf{x}} C_0) \quad \text{for } \mathbf{y} \in \partial\omega_b(\mathbf{x}),$$

$$(13e) \quad c_1 \text{ periodic} \quad \text{for } \mathbf{y} \in \partial\omega.$$

We may express the solutions to (13) in the form

$$(14a) \quad c_1(\mathbf{x}, \mathbf{y}, t) = -\boldsymbol{\xi}(\mathbf{x}, \mathbf{y}) \cdot \nabla_{\mathbf{x}} c_0(\mathbf{x}, t) + \check{c}_1(\mathbf{x}, t),$$

$$338 \quad (14b) \quad C_1(\mathbf{x}, \mathbf{y}, t) = -\Xi(\mathbf{x}, \mathbf{y}) \cdot \nabla_{\mathbf{x}} C_0(\mathbf{x}, t) + \check{C}_1(\mathbf{x}, t),$$

341 where \check{c}_1 and \check{C}_1 are (thus far) arbitrary functions of \mathbf{x} and t only, which we shall not
 342 need to calculate to obtain the leading-order homogenized problem. The components
 343 ξ_i and Ξ_i of the zero-mean (over a single cell) functions ξ and Ξ satisfy the cell
 344 problems

$$345 \quad (15a) \quad 0 = \nabla_{\mathbf{y}}^2 \xi_i \quad \text{for } \mathbf{y} \in \omega_m(\mathbf{x}),$$

$$346 \quad (15b) \quad 0 = D \nabla_{\mathbf{y}}^2 \Xi_i \quad \text{for } \mathbf{y} \in \omega_b(\mathbf{x}),$$

$$347 \quad (15c) \quad \xi_i = \Xi_i \quad \text{for } \mathbf{y} \in \partial\omega_b(\mathbf{x}),$$

$$348 \quad (15d) \quad \mathbf{n}_{\mathbf{y}} \cdot (\nabla_{\mathbf{y}} \xi_i - D \nabla_{\mathbf{y}} \Xi_i) = (1 - D) \mathbf{n}_{\mathbf{y}} \cdot \mathbf{e}_i \quad \text{for } \mathbf{y} \in \partial\omega_b(\mathbf{x}),$$

$$349 \quad (15e) \quad \xi_i \text{ periodic} \quad \text{for } \mathbf{y} \in \partial\omega,$$

351 where \mathbf{e}_i is the unit vector in the y_i -direction.

352 Finally, from the relevant $O(\epsilon^2)$ terms in (9), we obtain

$$353 \quad (16a) \quad \frac{\partial c_0}{\partial t} = \nabla_{\mathbf{y}} \cdot (\nabla_{\mathbf{y}} c_2 + \nabla_{\mathbf{x}} c_1) + \nabla_{\mathbf{x}} \cdot (\nabla_{\mathbf{y}} c_1 + \nabla_{\mathbf{x}} c_0) \quad \text{for } \mathbf{y} \in \omega_m(\mathbf{x}),$$

$$(16b)$$

$$354 \quad \frac{\partial C_0}{\partial t} = D \nabla_{\mathbf{y}} \cdot (\nabla_{\mathbf{y}} C_2 + \nabla_{\mathbf{x}} C_1) + D \nabla_{\mathbf{x}} \cdot (\nabla_{\mathbf{y}} C_1 + \nabla_{\mathbf{x}} C_0) - D \mu C_0 \quad \text{for } \mathbf{y} \in \omega_b(\mathbf{x}),$$

$$355 \quad (16c) \quad c_2 = C_2 \quad \text{for } \mathbf{y} \in \partial\omega_b(\mathbf{x}),$$

$$356 \quad \mathbf{n}_{\mathbf{y}} \cdot (\nabla_{\mathbf{y}} c_2 + \nabla_{\mathbf{x}} c_1) - \nabla_{\mathbf{x}} R \cdot (\nabla_{\mathbf{y}} c_1 + \nabla_{\mathbf{x}} c_0)$$

$$357 \quad (16d) \quad = D (\mathbf{n}_{\mathbf{y}} \cdot (\nabla_{\mathbf{y}} C_2 + \nabla_{\mathbf{x}} C_1) - \nabla_{\mathbf{x}} R \cdot (\nabla_{\mathbf{y}} C_1 + \nabla_{\mathbf{x}} C_0)) \quad \text{for } \mathbf{y} \in \partial\omega_b(\mathbf{x}),$$

$$358 \quad (16e) \quad c_2 \text{ periodic} \quad \text{for } \mathbf{y} \in \partial\omega.$$

360 To derive effective equations for the averaged concentrations defined in (6), we inte-
 361 grate (16a) over the domain $\omega_m(\mathbf{x})$ and (16b) over the domain $\omega_b(\mathbf{x})$, sum the results,
 362 then apply the divergence theorem with the boundary conditions (16d,e) to obtain

$$363 \quad \int_{\omega_m(\mathbf{x})} \frac{\partial c_0}{\partial t} d\mathbf{y} + \int_{\omega_b(\mathbf{x})} \frac{\partial C_0}{\partial t} d\mathbf{y} = \int_{\omega_m(\mathbf{x})} \nabla_{\mathbf{x}} \cdot (\nabla_{\mathbf{y}} c_1 + \nabla_{\mathbf{x}} c_0) d\mathbf{y}$$

$$364 \quad - \int_{\partial\omega_b(\mathbf{x})} \nabla_{\mathbf{x}} R \cdot (\nabla_{\mathbf{y}} c_1 + \nabla_{\mathbf{x}} c_0) ds + D \int_{\omega_b(\mathbf{x})} \nabla_{\mathbf{x}} \cdot (\nabla_{\mathbf{y}} C_1 + \nabla_{\mathbf{x}} C_0) d\mathbf{y}$$

$$365 \quad (17) \quad - D \int_{\partial\omega_b(\mathbf{x})} \nabla_{\mathbf{x}} R \cdot (\nabla_{\mathbf{y}} C_1 + \nabla_{\mathbf{x}} C_0) ds - D \mu \int_{\omega_b(\mathbf{x})} C_0 d\mathbf{y},$$

$$366$$

367 where ds is the surface element of the bacterial membrane $\partial\omega_b(\mathbf{x})$. Using the Reynolds
 368 transport theorem to combine the first and second integrals on the right-hand side of
 369 (17) as well as the third and fourth integrals, we obtain

$$370 \quad |\omega_m(\mathbf{x})| \frac{\partial c_0}{\partial t} + |\omega_b(\mathbf{x})| \frac{\partial C_0}{\partial t} = \nabla_{\mathbf{x}} \cdot \int_{\omega_m(\mathbf{x})} (\nabla_{\mathbf{y}} c_1 + \nabla_{\mathbf{x}} c_0) d\mathbf{y}$$

$$371 \quad (18) \quad + D \nabla_{\mathbf{x}} \cdot \int_{\omega_b(\mathbf{x})} (\nabla_{\mathbf{y}} C_1 + \nabla_{\mathbf{x}} C_0) d\mathbf{y} - D \mu |\omega_b(\mathbf{x})| C_0,$$

$$372$$

373 as the solvability condition required to close the leading-order problem. We note that
 374 $|\omega_m| + |\omega_b| = 1$, and that $|\omega_b| = 4\pi R^3/3$ for the spherical bacteria we consider in this
 375 paper.

376 We can use (14) to deduce that $\nabla_{\mathbf{y}}c_1 = -(\mathbf{J}_{\boldsymbol{\xi}}^T)\nabla_{\mathbf{x}}c_0$ and $\nabla_{\mathbf{y}}C_1 = -(\mathbf{J}_{\boldsymbol{\Xi}}^T)\nabla_{\mathbf{x}}C_0$,
 377 where $(\mathbf{J}_{\boldsymbol{\xi}}^T)_{ij} = \partial\xi_j/\partial y_i$ and $(\mathbf{J}_{\boldsymbol{\Xi}}^T)_{ij} = \partial\Xi_j/\partial y_i$ are the transposes of the Jacobian
 378 matrices of $\boldsymbol{\xi}$ and $\boldsymbol{\Xi}$, respectively, these being the vector solutions to the cell problems
 379 defined in (15). Using these results, recalling that $c_0 = C_0$ from the leading-order
 380 equations, and noting that the leading-order independence of c_0 on \mathbf{y} leads to the
 381 asymptotic result $\widehat{c} \sim c_0$ in (6a), we rewrite (18) as

$$382 \quad (19a) \quad \frac{\partial \widehat{c}}{\partial t} = \nabla_{\mathbf{x}} \cdot \left(\widehat{D}(\mathbf{x}) \nabla_{\mathbf{x}} \widehat{c} \right) - \frac{4}{3} \pi D \mu R^3 \widehat{c},$$

384 at leading order, with the initial condition

$$385 \quad (19b) \quad \widehat{c}(\mathbf{x}, 0) = c_{\text{init}}(\mathbf{x}),$$

387 obtained by substituting (12e) into (6a). The homogenized diffusion tensor is defined
 388 as

$$389 \quad (19c) \quad \widehat{D}(\mathbf{x})\mathbf{I} = \int_{\omega_m(\mathbf{x})} (\mathbf{I} - \mathbf{J}_{\boldsymbol{\xi}}^T) \, d\mathbf{y} + D \int_{\omega_b(\mathbf{x})} (\mathbf{I} - \mathbf{J}_{\boldsymbol{\Xi}}^T) \, d\mathbf{y},$$

391 and \mathbf{I} is the three-dimensional identity matrix. In the case of spherical bacteria, the
 392 homogenized diffusion tensor is a multiple of the identity matrix due to the symmetry
 393 of the cell problem (15). That is,

$$(20) \quad \int_{\omega_m(\mathbf{x})} \mathbf{J}_{\boldsymbol{\xi}}^T \, d\mathbf{y} = \left(\int_{\omega_m(\mathbf{x})} \partial\xi_i/\partial y_i \, d\mathbf{y} \right) \mathbf{I}, \quad \int_{\omega_b(\mathbf{x})} \mathbf{J}_{\boldsymbol{\Xi}}^T \, d\mathbf{y} = \left(\int_{\omega_b(\mathbf{x})} \partial\Xi_j/\partial y_j \, d\mathbf{y} \right) \mathbf{I},$$

396 for $i, j = 1, 2, 3$, with ξ_i and Ξ_j determined by (15). We are able to obtain analytic
 397 bounds on the effective diffusion coefficient using the Voigt-Reiss inequality (eq (1.63)
 398 in [19]), yielding

$$399 \quad (21) \quad \frac{D}{|\omega_b| + D|\omega_m|} \leq \widehat{D} \leq |\omega_m| + D|\omega_b|,$$

401 where we have used $|\omega| = 1$.

402 We note that \widehat{D} is a function of two parameters in this problem: the diffusion
 403 ratio D , and the bacterium radius R . We solve the cell problem (15) using the soft-
 404 ware package COMSOL Multiphysics to determine the effective diffusion coefficients,
 405 leading to the results in figure 2. As physically expected, when diffusion is slower
 406 within the bacteria than in the passive medium, the effective diffusion is slower than
 407 the pointwise diffusion in the passive medium, and *vice versa* for a quicker diffusion
 408 within the bacteria. Moreover, this effect is greater when the bacterial volume is
 409 larger. We note that when $D = 1$, the solutions to the cell problem (15) are indepen-
 410 dent of \mathbf{y} , resulting in $\widehat{D} \equiv 1$.

411 For our main goal of analysing the effective uptake, we see from (19a) that, in
 412 Case 1, the effective uptake is equal to the product of the pointwise uptake and the
 413 bacterial volume. For our additional aim of obtaining an equation for the averaged
 414 concentration $\bar{c}(\mathbf{x}, t)$, we note that the leading-order behaviour of (6b) is given by

$$415 \quad (22) \quad \bar{c}(\mathbf{x}, t) \sim \widehat{c}(\mathbf{x}, t).$$

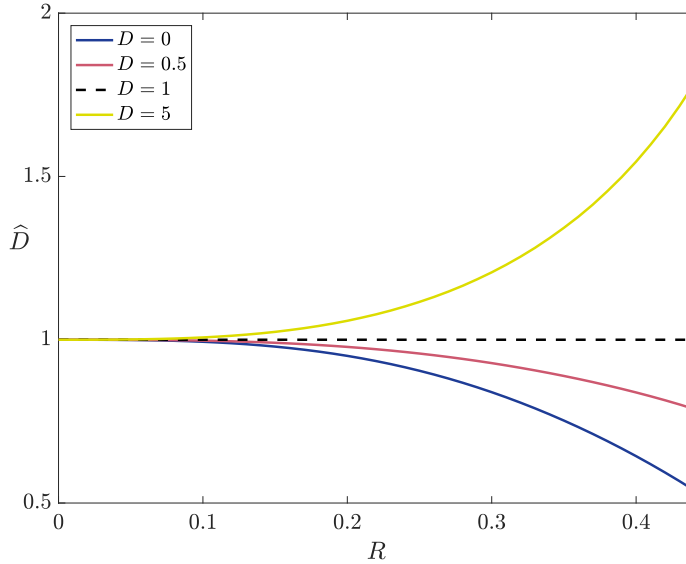


FIG. 2. The effective diffusion coefficient derived in Case 1, which is the distinguished asymptotic limit for the diffusion coefficient in the other cases we consider. The effective diffusion coefficient in Case 2 is given by the limit $D \rightarrow 0^+$, and the effective diffusion coefficient in Case 3 is given by the limit $R \rightarrow 0^+$. That is, in Case 3 the effective dimensionless diffusion coefficient is unity.

417 Thus, from (19) we deduce that the effective governing equation for \bar{c} is

418 (23a)
$$\frac{\partial \bar{c}}{\partial t} = \nabla_{\mathbf{x}} \cdot \left(\widehat{D}(\mathbf{x}) \nabla_{\mathbf{x}} \bar{c} \right) - \frac{4}{3} \pi D \mu R^3 \bar{c},$$

419

420 with initial condition

421 (23b)
$$\bar{c}(\mathbf{x}, 0) = c_{\text{init}}(\mathbf{x}),$$

423 obtained by substituting (12e) and (12f) into (6b). The generalization of this result
424 to arbitrary bacterial shapes is briefly discussed in Appendix A.

425 The effective governing equation (19) holds for $O(1)$ values of μ and D . However,
426 when μ is large and D is small, with $\mu D = O(1)$, the effective equation (19) is
427 not correct over an $O(1)$ timescale. We could anticipate the significant change in
428 behaviour in this limit from the terms in (9) switching asymptotic orders, and we
429 explore this limit in the next section.

430 **3.2. Case 2 - small diffusion, large uptake, and standard obstacle size:**

431 $D = O(\epsilon^2)$, $\mu = O(1/\epsilon^2)$, $R = O(1)$. The second distinguished limit we consider is
432 $D = O(\epsilon^2)$, $\mu = O(1/\epsilon^2)$, and $R = O(1)$. We consider this limit by setting $D = \epsilon^2 \widehat{D}$
433 and $\mu = \widehat{\mu}/\epsilon^2$, where \widehat{D} and $\widehat{\mu}$ are both of $O(1)$. As there is a large difference
434 between the diffusion coefficients in the medium and bacterium, this is a double-
435 porosity model. As discussed in §1, such models tend to induce a memory effect
436 in the upscaled effective equations, whereby the history of the system is required to
437 determine the current state of the system. We will find a similar effect in this case,
438 the partial differential equations being upscaled into integro-differential equations.

439 We introduce the asymptotic expansions

440 (24)
$$c = c_0(\mathbf{x}, \mathbf{y}, t) + \epsilon c_1(\mathbf{x}, \mathbf{y}, t) + \epsilon^2 c_2(\mathbf{x}, \mathbf{y}, t) + O(\epsilon^3), \quad C = C_0(\mathbf{x}, \mathbf{y}, t) + O(\epsilon),$$

441

442 to the governing equations (9), noting that we will only require the leading-order term
443 in C for the following analysis. The leading-order terms in (9) are

$$444 \quad (25a) \quad 0 = \nabla_{\mathbf{y}}^2 c_0 \quad \text{for } \mathbf{y} \in \omega_m(\mathbf{x}),$$

$$445 \quad (25b) \quad \frac{\partial C_0}{\partial t} = \hat{D} (\nabla_{\mathbf{y}}^2 C_0 - \hat{\mu} C_0) \quad \text{for } \mathbf{y} \in \omega_b(\mathbf{x}),$$

$$446 \quad (25c) \quad c_0 = C_0 \quad \text{for } \mathbf{y} \in \partial\omega_b(\mathbf{x}),$$

$$447 \quad (25d) \quad \mathbf{n}_{\mathbf{y}} \cdot \nabla_{\mathbf{y}} c_0 = 0 \quad \text{for } \mathbf{y} \in \partial\omega_b(\mathbf{x}),$$

$$448 \quad (25e) \quad c_0(\mathbf{x}, \mathbf{y}, 0) = c_{\text{init}}(\mathbf{x}) \quad \text{for } \mathbf{y} \in \omega_m(\mathbf{x}),$$

$$449 \quad (25f) \quad C_0(\mathbf{x}, \mathbf{y}, 0) = c_{\text{init}}(\mathbf{x}) \quad \text{for } \mathbf{y} \in \omega_b(\mathbf{x}),$$

$$450 \quad (25g) \quad c_0 \text{ periodic} \quad \text{for } \mathbf{y} \in \partial\omega.$$

452 The system for c_0 is defined by (25a,d,e,g), and decouples from C_0 . We see that c_0
453 is independent of \mathbf{y} , and thus $c_0 = c_0(\mathbf{x}, t)$ with $c_0(\mathbf{x}, 0) = c_{\text{init}}(\mathbf{x})$. We solve for C_0
454 later in this section.

455 The important $O(\epsilon)$ problem is for c_1 , for which we obtain the following system

$$456 \quad (26a) \quad 0 = \nabla_{\mathbf{y}}^2 c_1 \quad \text{for } \mathbf{y} \in \omega_m(\mathbf{x}),$$

$$457 \quad (26b) \quad \mathbf{n}_{\mathbf{y}} \cdot \nabla_{\mathbf{y}} c_1 = -\mathbf{n}_{\mathbf{y}} \cdot \nabla_{\mathbf{x}} c_0 \quad \text{for } \mathbf{y} \in \partial\omega_b(\mathbf{x}),$$

$$458 \quad (26c) \quad c_1 \text{ periodic} \quad \text{for } \mathbf{y} \in \partial\omega.$$

460 The system (26) is equivalent to taking the limit of $D \rightarrow 0$ in (13). Moreover, it is
461 the same first-correction problem that arises in [5, 11]. In a similar manner to the
462 analysis in §3.1, we may solve (26) by setting

$$463 \quad (27) \quad c_1(\mathbf{x}, \mathbf{y}, t) = -\gamma(\mathbf{x}, \mathbf{y}) \cdot \nabla_{\mathbf{x}} c_0(\mathbf{x}, t) + \check{c}(\mathbf{x}, t),$$

465 where \check{c} is an arbitrary function of \mathbf{x} and t only, and the components γ_i of the zero-
466 mean (over a single cell) function γ satisfy the cell problem

$$467 \quad (28a) \quad 0 = \nabla_{\mathbf{y}}^2 \gamma_i \quad \text{for } \mathbf{y} \in \omega_m(\mathbf{x}),$$

$$468 \quad (28b) \quad \mathbf{n}_{\mathbf{y}} \cdot \nabla_{\mathbf{y}} \gamma_i = \mathbf{n}_{\mathbf{y}} \cdot \mathbf{e}_i \quad \text{for } \mathbf{y} \in \partial\omega_b(\mathbf{x}),$$

$$469 \quad (28c) \quad \gamma_i \text{ periodic} \quad \text{for } \mathbf{y} \in \partial\omega,$$

471 where \mathbf{e}_i is the unit vector in the y_i -direction. The cell problem (28) for γ_i is equivalent
472 to the system (15) for ξ_i in the limit of $D \rightarrow 0$.

473 The relevant $O(\epsilon^2)$ problem is

$$474 \quad (29a) \quad \frac{\partial c_0}{\partial t} = \nabla_{\mathbf{y}} \cdot (\nabla_{\mathbf{y}} c_2 + \nabla_{\mathbf{x}} c_1) + \nabla_{\mathbf{x}} \cdot (\nabla_{\mathbf{y}} c_1 + \nabla_{\mathbf{x}} c_0) \quad \text{for } \mathbf{y} \in \omega_m(\mathbf{x}),$$

$$475 \quad (29b) \quad \mathbf{n}_{\mathbf{y}} \cdot (\nabla_{\mathbf{y}} c_2 + \nabla_{\mathbf{x}} c_1) - \nabla_{\mathbf{x}} R \cdot (\nabla_{\mathbf{y}} c_1 + \nabla_{\mathbf{x}} c_0) = \mathbf{n}_{\mathbf{y}} \cdot \hat{D} \nabla_{\mathbf{y}} C_0 \quad \text{for } \mathbf{y} \in \partial\omega_b(\mathbf{x}),$$

$$476 \quad (29c) \quad c_2 \text{ periodic} \quad \text{for } \mathbf{y} \in \partial\omega.$$

478 To derive effective equations for the averaged concentrations defined in (6), we proceed
479 in a similar manner to §3.1. We integrate (29a) over the domain $\omega_m(\mathbf{x})$, apply the
480 divergence theorem, and use the boundary conditions (29b,c) to obtain

$$481 \quad \int_{\omega_m(\mathbf{x})} \frac{\partial c_0}{\partial t} d\mathbf{y} = \int_{\omega_m(\mathbf{x})} \nabla_{\mathbf{x}} \cdot (\nabla_{\mathbf{y}} c_1 + \nabla_{\mathbf{x}} c_0) d\mathbf{y} - \int_{\partial\omega_b(\mathbf{x})} \nabla_{\mathbf{x}} R \cdot (\nabla_{\mathbf{y}} c_1 + \nabla_{\mathbf{x}} c_0) ds$$

482 (30)
$$- \int_{\partial\omega_b(\mathbf{x})} \mathbf{n}_y \cdot \hat{D} \nabla_y C_0 \, ds.$$

483

484 Using the Reynolds transport theorem to combine the first two integrals on the right-
485 hand side of (30), we obtain

486 (31)
$$|\omega_m(\mathbf{x})| \frac{\partial c_0}{\partial t} = \nabla_{\mathbf{x}} \cdot \int_{\omega_m(\mathbf{x})} (\nabla_y c_1 + \nabla_{\mathbf{x}} c_0) \, d\mathbf{y} - \hat{D} |\partial\omega_b(\mathbf{x})| \frac{\partial C_0}{\partial r} \Big|_{r=R}.$$

487

488 We use (27) to determine that $\nabla_y c_1 = -(\mathbf{J}_\gamma^T) \nabla_{\mathbf{x}} c_0$, where $(\mathbf{J}_\gamma^T)_{ij} = \partial\gamma_j/\partial y_i$ is the
489 transpose of the Jacobian matrix of γ , the vector solution to the cell problems defined
490 in (28). In the same manner as the previous case, we note that $\int_{\omega_m(\mathbf{x})} \mathbf{J}_\gamma^T \, d\mathbf{y} =$
491 $(\int_{\omega_m(\mathbf{x})} \partial\gamma_i/\partial y_i \, d\mathbf{y}) \mathbf{I}$ for $i = 1, 2, 3$ with γ_i determined in (28), allowing us to write
492 (31) as

493 (32)
$$|\omega_m(\mathbf{x})| \frac{\partial c_0}{\partial t} = \nabla_{\mathbf{x}} \cdot (|\omega_m| \overline{D}(\mathbf{x}) \nabla_{\mathbf{x}} c_0) - \hat{D} |\partial\omega_b(\mathbf{x})| \frac{\partial C_0}{\partial r} \Big|_{r=R},$$

494

495 where the classical homogenized diffusion tensor is defined as

496 (33)
$$\overline{D}(\mathbf{x}) \mathbf{I} = \left(\mathbf{I} - \frac{1}{|\omega_m|} \int_{\omega_m(\mathbf{x})} \mathbf{J}_\gamma^T \, d\mathbf{y} \right).$$

497

498 The effective diffusion coefficient \overline{D} we obtain here is identical to the effective dif-
499 fusion coefficients derived in [5] and [11] for diffusion past impermeable spheres in
500 a cubic array with no adsorption and surface adsorption, respectively (advection is
501 also considered in [11]). This is because we have considered the small diffusivity limit
502 within the bacteria, making the obstacles appear impermeable at leading order. We
503 show this effective diffusion coefficient in figure 2, as \overline{D} is equivalent to \hat{D} when $D = 0$
504 in the latter. Thus, the effective diffusion coefficient in Case 2 is a sublimit of the
505 effective diffusion coefficient in Case 1.

506 To obtain a governing equation for \hat{c} from (32), we first note that $\hat{c} \sim c_0$ in (6a).
507 This arises from the leading-order independence of c_0 on \mathbf{y} . Using (25b) and (25f),
508 we can write (32) as

509 (34)
$$\frac{\partial}{\partial t} \left(|\omega_m(\mathbf{x})| \hat{c} + \int_{\omega_b(\mathbf{x})} C_0(\mathbf{x}, \mathbf{y}, t) \, d\mathbf{y} \right) = \nabla_{\mathbf{x}} \cdot (|\omega_m| \overline{D}(\mathbf{x}) \nabla_{\mathbf{x}} \hat{c}) - \hat{\mu} \hat{D} \int_{\omega_b(\mathbf{x})} C_0(\mathbf{x}, \mathbf{y}, t) \, d\mathbf{y},$$

510

511 where C_0 depends on \hat{c} through the leading-order problem

512 (35a)
$$\frac{\partial C_0}{\partial t} = \hat{D} (\nabla_y^2 C_0 - \hat{\mu} C_0) \quad \text{for } \mathbf{y} \in \omega_b(\mathbf{x}),$$

513 (35b)
$$C_0 = \hat{c}(\mathbf{x}, t) \quad \text{for } \mathbf{y} \in \partial\omega_b(\mathbf{x}),$$

514 (35c)
$$C_0(\mathbf{x}, \mathbf{y}, 0) = c_{\text{init}}(\mathbf{x}) \quad \text{for } \mathbf{y} \in \omega_b(\mathbf{x}).$$

515

516 We seek a radially symmetric solution for C_0 (in terms of $r = \|\mathbf{y}\|$), imposing
517 $\partial C_0/\partial r = 0$ at $r = 0$ to ensure boundedness at the origin, and find a representa-
518 tion of the solution in the form

519 (36a)
$$C_0(\mathbf{x}, r, t) = \hat{c}(\mathbf{x}, t) + \frac{1}{r} \sum_{n=1}^{\infty} U_n(\mathbf{x}, t) \sin a_n r,$$

$$520 \quad (36b) \quad U_n(\mathbf{x}, t) = e^{-\hat{D}(\hat{\mu}+a_n^2)t} \frac{2(-1)^n}{a_n} \int_0^t \left(\frac{\partial \hat{c}}{\partial \tau} + \hat{\mu} \hat{D} \hat{c}(\mathbf{x}, \tau) \right) e^{\hat{D}(\hat{\mu}+a_n^2)\tau} d\tau,$$

$$521 \quad (36c) \quad a_n(\mathbf{x}) = \frac{n\pi}{R(\mathbf{x})},$$

523 where a_n represents the eigenvalues of the time-dependent problem. Integrating by
524 parts the first term in the integrand of (36b) and re-writing the first term in (36a)
525 in terms of a Fourier series in $\sin a_n r$ (essentially encoding $-\hat{c}$ multiplied by a sign
526 function translated to have origin at $r = R$), we can also write

$$527 \quad (37) \quad C_0(\mathbf{x}, r, t) = -\frac{2}{r} \sum_{n=1}^{\infty} (-1)^n e^{-\hat{D}(\hat{\mu}+a_n^2)t} \left(\frac{c_{\text{init}}(\mathbf{x})}{a_n} + \hat{D} a_n \int_0^t \hat{c}(\mathbf{x}, \tau) e^{\hat{D}(\hat{\mu}+a_n^2)\tau} d\tau \right) \sin a_n r,$$

529 where the boundary condition (35b) is now satisfied as $r \rightarrow R^-$.

530 Noting that $|\omega_m| = 1 - 4\pi R^3/3$ for spherical bacteria, we use (36) to write (34)
531 as the homogenized equation

$$532 \quad (38a) \quad \frac{\partial \hat{c}}{\partial t} = \nabla_{\mathbf{x}} \cdot \left(\left(1 - \frac{4}{3}\pi R^3 \right) \bar{D}(\mathbf{x}) \nabla_{\mathbf{x}} \hat{c} \right) - f[\hat{c}],$$

534 with the initial condition

$$535 \quad (38b) \quad \hat{c}(\mathbf{x}, 0) = c_{\text{init}}(\mathbf{x}),$$

537 obtained by substituting (25e) into (6a), and where $f[\cdot]$ denotes that the effective
538 uptake is a (non-local) functional, defined as

$$539 \quad (38c) \quad f[\hat{c}] = 8\pi R \hat{D} \sum_{n=1}^{\infty} \left\{ e^{-\hat{D}(\hat{\mu}+a_n^2)t} \int_0^t \left(\frac{\partial \hat{c}}{\partial \tau} + \hat{\mu} \hat{D} \hat{c}(\mathbf{x}, \tau) \right) e^{\hat{D}(\hat{\mu}+a_n^2)\tau} d\tau \right\} - \frac{4}{3}\pi R^3 \frac{\partial \hat{c}}{\partial t}.$$

541 Thus, we have an effective integro-differential equation for the leading-order intrinsic-
542 averaged concentration. We note that the effective uptake is now significantly more
543 complicated than for Case 1, and will depend on the initial conditions of the problem,
544 but is still of $O(1)$.

545 We can also determine an equation for the volumetric-averaged concentration,
546 defined in (6b), in terms of the intrinsic-averaged concentration. Substituting the
547 asymptotic expansions (24) and leading-order solution (37) into the definition of the
548 effective concentration (6b), we deduce that \bar{c} can be calculated from \hat{c} using the
549 relationship

$$550 \quad (39) \quad \bar{c} \sim \left(1 - \frac{4}{3}\pi R^3 \right) \hat{c} + 8\pi R \sum_{n=1}^{\infty} e^{-\hat{D}(\hat{\mu}+a_n^2)t} \left(\frac{c_{\text{init}}(\mathbf{x})}{a_n^2} + \hat{D} \int_0^t \hat{c}(\mathbf{x}, s) e^{\hat{D}(\hat{\mu}+a_n^2)\tau} d\tau \right).$$

552 For certain types of boundary condition (e.g. Dirichlet, Robin, or mixed) on
553 the boundary of Ω , it is possible to obtain a nontrivial steady solution to (38) and
554 (39). It is simpler to analyse the effective uptake for Case 2 in the steady rather than
555 the unsteady state, as the effective governing equation is reduced from an integro-
556 differential equation to the elliptic partial differential equation

$$557 \quad (40a) \quad 0 = \nabla_{\mathbf{x}} \cdot \left(\left(1 - \frac{4}{3}\pi R^3 \right) \bar{D}(\mathbf{x}) \nabla_{\mathbf{x}} \hat{c} \right) - \sigma \hat{c},$$

558

559 where

$$560 \quad (40b) \quad \sigma = 4\pi R \hat{D} \left(\sqrt{\hat{\mu}} R \coth \sqrt{\hat{\mu}} R - 1 \right),$$

561

562 using the identity

$$563 \quad (41) \quad \sum_{n=1}^{\infty} \frac{1}{\alpha + n^2 \pi^2} = \frac{\sqrt{\alpha} \coth \sqrt{\alpha} - 1}{2\alpha},$$

564

565 to reduce $f[\hat{c}]$ to a linear function of \hat{c} , in the steady state. We could also obtain (40a)
 566 by direct consideration of the steady version of (25). Additionally, we find that if \hat{c}
 567 tends to a constant as $t \rightarrow \infty$, (39) reduces to

$$568 \quad (42) \quad \bar{c} \sim \left(1 - \frac{4}{3} \pi R^3 \right) \hat{c} + \frac{\sigma}{\hat{\mu} \hat{D}} \hat{c},$$

569

570 again using (41).

571 The steady state effective uptake coefficient in Case 2 is given by (40b). It is
 572 helpful to understand the sublimits of this coefficient in the steady regime before
 573 discussing the unsteady regime. For small $\sqrt{\hat{\mu}} R$, we see that

$$574 \quad (43a) \quad \sigma \sim \frac{4}{3} \pi \hat{\mu} \hat{D} R^3,$$

575

576 the bacterium volume multiplied by the pointwise uptake rate within a bacterium.
 577 This volume scaling is the same effective uptake we derived in Case 1. For large $\sqrt{\hat{\mu}} R$,
 578 we deduce that

$$579 \quad (43b) \quad \sigma \sim 4\pi R \hat{D} (\sqrt{\hat{\mu}} R - 1) \sim 4\pi \sqrt{\hat{\mu}} \hat{D} R^2,$$

580

581 the product of the bacterium surface area, the pointwise uptake rate, and $1/\sqrt{\hat{\mu}}$, the
 582 width of an uptake boundary layer for large $\hat{\mu}$ near the bacterial membrane. Thus, the
 583 effective uptake function we have derived in (38c) provides the function that smoothly
 584 transitions between volume-scaled and surface-area-scaled effective bacterial uptake.
 585 We illustrate these results in figure 3. We consider the generalization of these results
 586 to arbitrary bacterial shapes in Appendix A. In particular, we note that the physical
 587 intuition and subsequent scalings for the large pointwise uptake result given in (43b)
 588 generalizes for an arbitrary shape.

589 Although our main goal in this paper is to derive the effective uptake within a
 590 colony of bacteria, it is interesting to briefly consider $\hat{\mu} < 0$, corresponding to auto-
 591 catalytic production of some chemical within the bacteria or positive autoregulation
 592 of gene expression. As $\hat{\mu}$ decreases, the steady state equation (40) yields a blow-up in
 593 the effective production rate when

$$594 \quad (44) \quad \hat{\mu} = -\pi^2/R^2.$$

595

596 Thus, we may conclude that our results are only valid for negative $\hat{\mu}$ when $\hat{\mu} >$
 597 $-\pi^2/R^2$. Additionally, although the chemical production is self-promoting in this
 598 scenario, a steady state is still possible when the above inequality is satisfied.

599 In the unsteady regime, governed by the full homogenized system (38), we see that
 600 the effective uptake has a natural timescale of $O(1/\hat{D})$ for extreme values of \hat{D} . Thus,

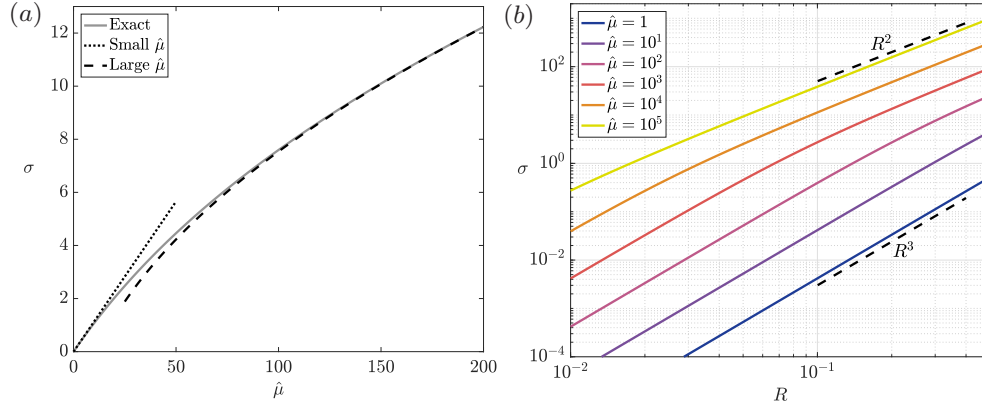


FIG. 3. The steady-state effective uptake coefficient σ in Case 2, given by (40b) as a function of (a) $\hat{\mu}$ (with $\hat{D} = 1$ and $R = 0.3$) and (b) R (with $\hat{D} = 1$). In (a), we show that $\sigma \sim 4\pi R^3 \hat{D} \hat{\mu} / 3$ for small $\hat{\mu}$ and $\sigma \sim 4\pi R \hat{D} (\sqrt{\hat{\mu} R} - 1)$ for large $\hat{\mu}$, as shown in (43). In (b), we show that σ scales with R^3 for small $\sqrt{\hat{\mu} R}$ and with R^2 for large $\sqrt{\hat{\mu} R}$.

601 small and large \hat{D} in (38) correspond to slow and fast uptake, respectively. In the
 602 limit of small \hat{D} , the leading-order intrinsic-averaged concentration becomes spatially
 603 independent over a timescale of $O(1/\hat{D})$, where the slow uptake is a function of time
 604 forced by (38c). The volumetric-averaged concentration is still given by the full form
 605 of (39). In the limit of large \hat{D} , the initial conditions quickly become unimportant and
 606 the effective uptake $f[\hat{c}]$ reduces from a functional in \hat{c} to the linear function $\nu \hat{c}$, defined
 607 in (40). This occurs because the fast diffusion removes the memory property from
 608 the upscaled problem. In the same manner, the volumetric-averaged concentration
 609 (39) tends to its steady-state value (42) over a timescale of $O(1/\hat{D})$ in this limit. A
 610 small $\hat{\mu}$ corresponds to slow uptake within the bacteria. In this limit, the unsteady
 611 concentration transport is governed by diffusion at leading order, before eventually
 612 tending to the small effective uptake given in (43a). A large $\hat{\mu}$ corresponds to quick
 613 uptake, and in this case the effective uptake $f[\hat{c}]$ reduces from a functional in \hat{c} to the
 614 linear function $\nu \hat{c}$, in the same manner as for large \hat{D} .

615 We note that taking the double limits of large \hat{D} and small $\hat{\mu}$ commute, yielding an
 616 effective uptake of $4\pi R^3 \hat{D} \hat{\mu} \hat{c} / 3$, which coincides with the effective uptake we derived
 617 in Case 1. Moreover, in the same limit, the upscaled governing equation (38) for Case
 618 2 coincides with the upscaled governing equation (19) for Case 1, in the limit of D
 619 being small. Thus, we are able to smoothly pass between Cases 1 and 2 and, in fact,
 620 the effective uptake in Case 1 is a sublimit of the effective uptake in Case 2 and the
 621 effective diffusion in Case 2 is a sublimit of the effective diffusion in Case 1.

622 Each of the limiting results we discuss above could have been directly calculated
 623 by taking their respective limits before the homogenization procedure, but our method
 624 produces a distinguished limit from which the relevant sublimits can be distilled, as
 625 long as $R = O(1)$. In the next section, we consider the final distinguished limit, which
 626 occurs when R is small and μ is very large.

627 **3.3. Case 3 - standard diffusion, very large uptake, and small obstacle**
 628 **size:** $D = O(1)$, $\mu = O(1/\epsilon^6)$, $R = O(\epsilon^2)$.

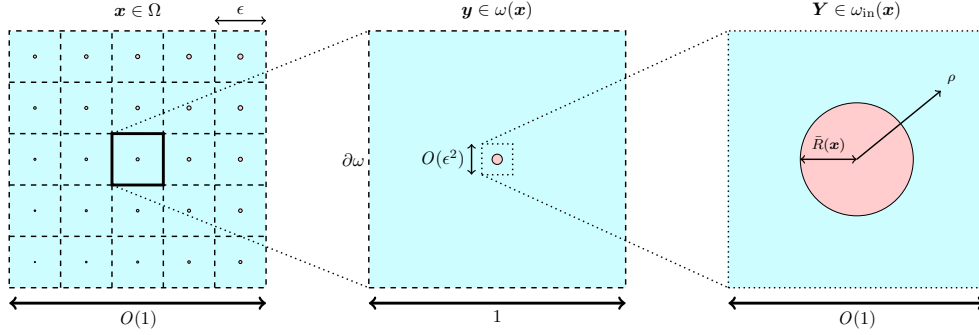


FIG. 4. A two-dimensional projection of the asymptotic structure of the three-dimensional problem with small obstacles. The full problem is shown in the left figure, the centre figure denotes the cell problem (with $\mathbf{y} \in [-1/2, 1/2]^3$), and the rightmost figure denotes the inner problem within the cell problem (with $\mathbf{Y} \in \mathbb{R}^3$ and $\rho = \|\mathbf{Y}\|$). In the cell problem, the effect of the bacterial sink occurs through a delta function, and not through its geometry. The strength of this sink is determined by solving the inner problem.

629 **3.3.1. Asymptotic structure.** We now consider the problem where $R \ll 1$,
630 by investigating the distinguished limit $R = O(\epsilon^2)$, $\mu = O(1/\epsilon^6)$, and $D = O(1)$.
631 Note that we have previously scaled R with the microscale variable, so in terms
632 of dimensionless macroscale variables we are considering the case where the radius
633 scales with the cube of the small parameter of periodicity, the critical case in [8]. We
634 introduce $R = \epsilon^2 \bar{R}$ and $\mu = \bar{\mu}/\epsilon^6$, where \bar{R} and $\bar{\mu}$ are both of $O(1)$.

635 In this section, our analysis involves upscaling the governing equations (3) using
636 a combination of boundary layer analysis and homogenization via the method of mul-
637 tiple scales. There are three important asymptotic regions in this problem. The first
638 is the outer region, over which $\mathbf{x} = O(1)$. In the same manner as the previous two
639 cases, we wish to determine an upscaled effective equation over this region that sys-
640 tematically accounts for the bacterial uptake. Thus, in the outer region, the bacterial
641 uptake is a bulk effect. The second region is the cell region, over which $\mathbf{x} = O(\epsilon)$.
642 This region will yield the cell problem and, in this region, the bacterial uptake is a
643 point sink. The third and final region is the inner region, over which $\mathbf{x} = O(\epsilon^3)$.
644 In this region, we see the bacteria as an $O(1)$ region, within which we must solve a
645 concentration problem coupled to the passive medium. The solution from the inner
646 region determines the strength of the point sink in the cell region. Thus, this limit
647 introduces an additional term to the previous equations (9) with which we worked.
648 A schematic of these three regions is given in figure 4.

649 **3.3.2. Homogenization.** Re-writing the equations (9) in terms of the scaled
650 dimensionless parameters, we obtain

$$651 \quad (45a) \quad \epsilon^2 \frac{\partial c}{\partial t} = (\nabla_{\mathbf{y}} + \epsilon \nabla_{\mathbf{x}}) \cdot (\nabla_{\mathbf{y}} + \epsilon \nabla_{\mathbf{x}}) c \quad \text{for } \|\mathbf{y}\| > \epsilon^2 \bar{R} \text{ and } \|\mathbf{y}\|_{\infty} < 1/2,$$

$$652 \quad (45b) \quad \epsilon^6 \frac{\partial C}{\partial t} = \epsilon^4 D (\nabla_{\mathbf{y}} + \epsilon \nabla_{\mathbf{x}}) \cdot (\nabla_{\mathbf{y}} + \epsilon \nabla_{\mathbf{x}}) C - D \bar{\mu} C \quad \text{for } \|\mathbf{y}\| < \epsilon^2 \bar{R},$$

$$653 \quad (45c) \quad c = C \quad \text{for } \|\mathbf{y}\| = \epsilon^2 \bar{R},$$

$$654 \quad (45d) \quad (\mathbf{n}_{\mathbf{y}} - \epsilon \nabla_{\mathbf{x}} R) \cdot (\nabla_{\mathbf{y}} + \epsilon \nabla_{\mathbf{x}}) c = (\mathbf{n}_{\mathbf{y}} - \epsilon \nabla_{\mathbf{x}} R) \cdot D (\nabla_{\mathbf{y}} + \epsilon \nabla_{\mathbf{x}}) C \quad \text{for } \|\mathbf{y}\| = \epsilon^2 \bar{R},$$

$$655 \quad (45e) \quad c(\mathbf{x}, \mathbf{y}, 0) = c_{\text{init}}(\mathbf{x}) \quad \text{for } \|\mathbf{y}\| > \epsilon^2 \bar{R} \text{ and } \|\mathbf{y}\|_\infty < 1/2,$$

$$656 \quad (45f) \quad C(\mathbf{x}, \mathbf{y}, 0) = c_{\text{init}}(\mathbf{x}) \quad \text{for } \|\mathbf{y}\| < \epsilon^2 \bar{R},$$

$$657 \quad (45g) \quad c \text{ periodic} \quad \text{for } \|\mathbf{y}\|_\infty = 1/2.$$

659 We cannot obtain a solution for C by simply expanding in powers of ϵ , as we did for the
 660 previous two cases, since the bacterial domain in (45) depends on the small parameter
 661 ϵ . Instead, we seek an inner solution to the system near the small bacterium at the
 662 origin where $\|\mathbf{y}\| = O(\epsilon^2)$. In the next section, we show that the inner solution only
 663 affects the governing equation for c in the cell region at $O(\epsilon^2)$. Thus, substituting
 664 the asymptotic expansion $c(\mathbf{x}, \mathbf{y}, t) \sim c_0(\mathbf{x}, \mathbf{y}, t) + \epsilon c_1(\mathbf{x}, \mathbf{y}, t) + \epsilon^2 c_2(\mathbf{x}, \mathbf{y}, t)$ into (45a)
 665 implies that $c_0 = c_0(\mathbf{x}, t)$ and $c_1 = c_1(\mathbf{x}, t)$. We now investigate the inner region.

666 **3.3.3. Inner region.** We scale $\mathbf{y} = \epsilon^2 \mathbf{Y}$, where $\mathbf{Y} \in \mathbb{R}^3$. We define this inner
 667 region as $\omega_{\text{in}}(\mathbf{x})$, where the dependence on \mathbf{x} arises from the radius of the bacterium
 668 in this domain. From (45), the relevant leading-order system is

$$669 \quad (46a) \quad \nabla_{\mathbf{Y}}^2 c = O(\epsilon^6) \quad \text{for } \rho > \bar{R}(\mathbf{x}),$$

$$670 \quad (46b) \quad \nabla_{\mathbf{Y}}^2 C - \bar{\mu} C = O(\epsilon^6) \quad \text{for } \rho < \bar{R}(\mathbf{x}),$$

$$671 \quad (46c) \quad c = C \quad \text{for } \rho = \bar{R}(\mathbf{x}),$$

$$672 \quad (46d) \quad \frac{\partial c}{\partial \rho} = D \frac{\partial C}{\partial \rho} + O(\epsilon^3) \quad \text{for } \rho = \bar{R}(\mathbf{x}),$$

$$673 \quad (46e) \quad c \rightarrow c_0(\mathbf{x}, t) \quad \text{as } \rho \rightarrow \infty,$$

675 where $\rho = \|\mathbf{Y}\|$. The error estimate for (46d) arises from the slow variation in
 676 bacterium radius between neighbouring cells, which will play no significant role in
 677 this analysis. The far-field condition (46e) arises from matching with the cell region
 678 using van Dyke's matching principle [30]. We do not require the initial conditions for
 679 this case as we are only concerned with the problem when $t = O(1)$.

680 Imposing a vanishing concentration flux at the origin to ensure boundedness, the
 681 general radially symmetric solution to (46) is

$$682 \quad (47a) \quad c = c_0(\mathbf{x}, t) \left(1 - \frac{\bar{R} D}{\rho} \frac{\sqrt{\bar{\mu}} \bar{R} \coth \sqrt{\bar{\mu}} \bar{R} - 1}{1 + D (\sqrt{\bar{\mu}} \bar{R} \coth \sqrt{\bar{\mu}} \bar{R} - 1)} \right),$$

$$683 \quad (47b) \quad C = \frac{c_0(\mathbf{x}, t) \bar{R} \sinh \sqrt{\bar{\mu}} \rho}{\rho (D \sqrt{\bar{\mu}} \bar{R} \cosh \sqrt{\bar{\mu}} \bar{R} + (1 - D) \sinh \sqrt{\bar{\mu}} \bar{R})}.$$

685 To correctly match into the cell region, we write the $O(1)$ solution in the inner region
 686 (47) in terms of the cell region variables and expand to $O(\epsilon^2)$, yielding

$$687 \quad (48) \quad c \sim c_0(\mathbf{x}, t) - \epsilon^2 \frac{\nu}{4\pi \|\mathbf{y}\|} c_0(\mathbf{x}, t),$$

689 where

$$690 \quad (49) \quad \nu = \frac{4\pi \bar{R} D (\sqrt{\bar{\mu}} \bar{R} \coth \sqrt{\bar{\mu}} \bar{R} - 1)}{1 + D (\sqrt{\bar{\mu}} \bar{R} \coth \sqrt{\bar{\mu}} \bar{R} - 1)}.$$

692 The form of the matching condition (48) at $O(\epsilon^2)$ implies that the outer problem (45a)
 693 in the cell region with a boundary at $\|\mathbf{y}\| = \epsilon^2 \bar{R}$ can be replaced by an effective outer
 694 problem in the cell region, replacing the small bacterial boundary with a Dirac delta
 695 function at the origin of strength $-\epsilon^2 \nu c_0$. We now investigate this outer problem.

696 **3.3.4. Higher-order cell region problem.** Introducing the Dirac delta func-
697 tion formulation of the cell region problem (45), the $O(\epsilon^2)$ terms are

$$698 \quad (50a) \quad \frac{\partial c_0}{\partial t} = \nabla_{\mathbf{y}}^2 c_2 + \nabla_{\mathbf{x}}^2 c_0 - \nu \delta(\mathbf{y}) c_0 \quad \text{for } \mathbf{y} \in \omega,$$

$$699 \quad (50b) \quad c_0 \text{ periodic} \quad \text{for } \mathbf{y} \in \partial\omega,$$

701 where the introduction of a delta function is justified in the previous section.

702 Integrating (50a) over the cell, applying the periodic boundary conditions (50b),
703 and noting that (6) yields $\hat{c} \sim c_0$ at leading order, we obtain the effective equation
704 for the intrinsic-averaged concentration

$$705 \quad (51a) \quad \frac{\partial \hat{c}}{\partial t} = \nabla_{\mathbf{x}}^2 \hat{c} - \nu \hat{c}.$$

707 where ν is defined in (49), together with the initial condition

$$708 \quad (51b) \quad \hat{c}(\mathbf{x}, 0) = c_{\text{init}}(\mathbf{x}),$$

710 which arises by substituting (45e) into (6a). Moreover, as the bacteria are very small,
711 with $|\omega_b| = O(\epsilon^2)$, the volumetric-averaged concentration $\bar{c} \sim \hat{c}$, and thus (51) also
712 provides the homogenized system for \bar{c} . As with the previous cases, the effective
713 uptake is of $O(1)$, and for certain types of boundary condition (e.g. Dirichlet, Robin,
714 or mixed) on the boundary of Ω , it is possible to obtain a nontrivial steady solution to
715 (51). The effective diffusion coefficient here is unity, and thus the effective diffusion in
716 Case 3 is a sublimit of the effective diffusion in Case 1 as the bacterial radius becomes
717 small.

718 The effective uptake in Case 3 is given by $\nu \hat{c}$, defined in (49), and we now discuss
719 how this scales with the bacterial properties. In a similar manner to Case 2, the
720 parameter grouping $\sqrt{\bar{\mu}} \bar{R}$ is important. From (49), we see that a small $\sqrt{\bar{\mu}} \bar{R}$ yields

$$721 \quad (52) \quad \nu \sim \frac{4}{3} \pi D \bar{\mu} \bar{R}^3,$$

723 the bacterium volume multiplied by the pointwise uptake rate within a bacterium.
724 This is equivalent to (43a), the small uptake sublimit in Case 2, and thus is the same
725 effective uptake we derived in Case 1. For a small D , we see from (49) that

$$726 \quad (53) \quad \nu \sim 4\pi \bar{R} D (\sqrt{\bar{\mu}} \bar{R} \coth \sqrt{\bar{\mu}} \bar{R} - 1),$$

728 which is equivalent to the steady state effective uptake coefficient σ from Case 2.
729 This is because small D corresponds to bacteria that are much less permeable to
730 the nutrient, the scenario considered in Case 2, and we have preserved the scaling
731 $\epsilon^2 \bar{\mu} \bar{R}^2 = O(1)$ in both Cases 2 and 3. For large $\sqrt{\bar{\mu}} \bar{R}$ or large D , we deduce that

$$733 \quad (54) \quad \nu \sim 4\pi \bar{R},$$

734 which, notably, is bounded above as $\bar{\mu} \rightarrow \infty$. This is because the nutrient con-
735 centration within each bacterium is much smaller in Case 3 than in Cases 1 and 2.
736 Mathematically, for a large $\bar{\mu}$ in Case 3, the concentration within a bacterium is ap-
737 proximately $\hat{c}/(D\sqrt{\bar{\mu}}\bar{R})$ near the bacterial membrane over a region depth of $O(1/\sqrt{\bar{\mu}})$
738 (see (47)), whereas for large $\hat{\mu}$ in non-sparse bacteria, as considered in §3.2, the con-
739 centration within the bacterium scales with \hat{c} near the boundary over a region depth of

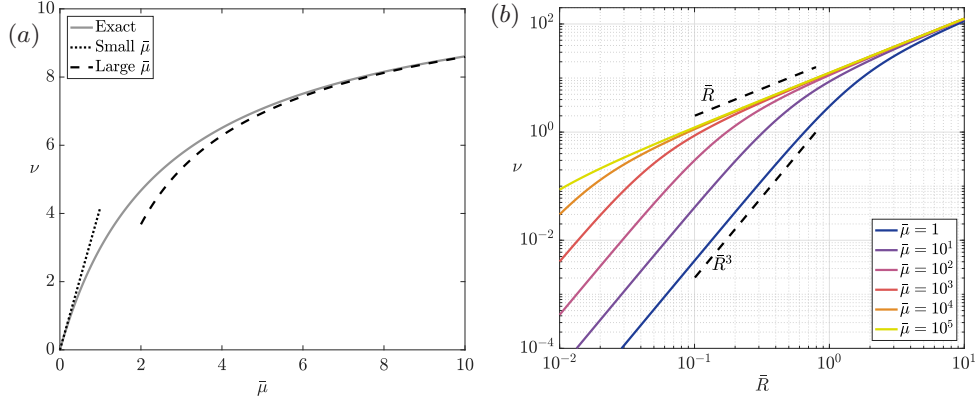


FIG. 5. The effective uptake coefficient ν in Case 3, given by (49), as a function of (a) $\bar{\mu}$ (with $D = 1$ and $\bar{R} = 1$) and (b) \bar{R} (with $D = 1$). In (a), we show that $\nu \sim 4\pi\bar{R}^3 D\bar{\mu}/3$ for small $\bar{\mu}$ and $\nu \sim 4\pi\bar{R}(1 - 1/(\sqrt{\bar{\mu}}D\bar{R}))$ for large $\bar{\mu}$. In (b), we show that ν scales with \bar{R}^3 for small $\sqrt{\bar{\mu}}\bar{R}$ and with \bar{R} for large $\sqrt{\bar{\mu}}\bar{R}$.

740 $O(1/\sqrt{\bar{\mu}})$. Thus, the concentration within each bacterium is reduced as $\bar{\mu}$ gets larger,
 741 in a manner that bounds above the effective uptake. We show these scalings in figure
 742 5. We consider the generalization of these results to arbitrary bacterial shapes in
 743 Appendix A. We show that the effective uptake becomes independent of $\bar{\mu}$ as $\bar{\mu} \rightarrow \infty$,
 744 and we are also able to obtain analytic results for ellipsoidal bacteria in the same
 745 limit.

746 As with Case 2, it is interesting to briefly consider $\bar{\mu} < 0$ in Case 3, corresponding
 747 to autocatalytic production of some chemical or positive autoregulation of gene ex-
 748 pression within the bacteria. As $\bar{\mu}$ decreases in this scenario, the effective production
 749 rate blows up in the homogenized equation (51) when

$$750 \quad (55) \quad \sqrt{-\bar{\mu}}\bar{R} \cot \sqrt{-\bar{\mu}}\bar{R} = \frac{D-1}{D}, \quad \text{for } \bar{\mu} \in (-\pi^2/\bar{R}^2, 0).$$

752 Thus, we may conclude that our homogenization results are only valid for negative $\bar{\mu}$
 753 when $\bar{\mu}$ is greater than the lower bound given by (55). We illustrate this lower bound
 754 in figure 6. Moreover, as with Case 2, we note that although the chemical production
 755 is self-promoting in this scenario, a steady state is still possible provided that $-\bar{\mu}$
 756 is not too large. This critical value depends on D and we find that, as D increases,
 757 $-\bar{\mu}$ is restricted to smaller maximum values for our homogenization results to hold. We
 758 additionally note that (44), the blow up in Case 2, is a sublimit of (55) for small D ,
 759 with appropriate scalings of $\bar{\mu}$ and \bar{R} .

760 Finally, we note that we can formally pass between Cases 1, 2, and 3. We can
 761 smoothly pass between Cases 1 and 3 by considering the limits where $R \rightarrow 0$ and
 762 $\mu \rightarrow \infty$ with $\mu R^3 = O(1)$ in Case 1, and the limit where $\bar{R} \rightarrow \infty$ and $\bar{\mu} \rightarrow 0$ with
 763 $\bar{\mu}\bar{R}^3 = O(1)$ in Case 3. Additionally, we can smoothly pass between Cases 2 and 3 by
 764 considering the limits where $R \rightarrow 0$ and $\hat{\mu} \rightarrow \infty$ with $\hat{\mu}R^2 = O(1)$ in Case 2, and the
 765 limit where $\bar{R} \rightarrow \infty$ and $D \rightarrow 0$ with $\bar{\mu}\bar{R}^2 = O(1)$ in Case 3. Thus, by considering
 766 the distinguished asymptotic limits, we have determined the different forms an $O(1)$
 767 effective uptake can take over a timescale of $O(1)$, corresponding to the timescale of
 768 diffusion over the macroscale.

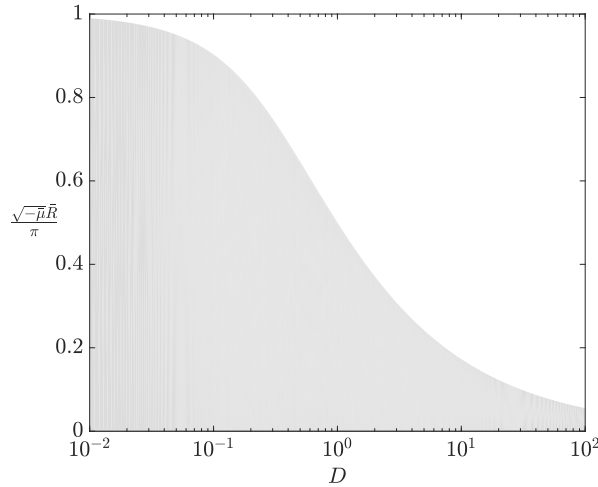


FIG. 6. The grey region denotes the lower bound of the domain of validity for negative $\bar{\mu}$, which corresponds to autocatalytic production or positive autoregulation of gene expression within the bacteria. The boundary between domains is defined by (55).

769 **4. Discussion.** We have systematically derived effective reaction–diffusion equa-
 770 tions from the microscale problem of unsteady diffusion of nutrient through a passive
 771 medium containing a locally periodic array of spherical bacteria. The nutrient can
 772 diffuse within these bacteria, which also act as volume sinks of the nutrient with
 773 first-order kinetics. We have shown that with only two mechanisms, diffusion and
 774 uptake, there are three distinguished limits where the effective uptake balances the
 775 macroscale diffusion over the timescale of the latter, and we have comprehensively
 776 investigate each limit. As we investigated spherical bacteria, we have been able to
 777 maximize our analytic progress and we have a closed-form expression for the effective
 778 uptake in each distinguished limit. We have been able to pass smoothly between
 779 each case as the system parameters vary, allowing us to determine how the effective
 780 uptake switches between scaling with the volume and surface area of the bacteria.
 781 Moreover, we have calculated the correct form of the effective uptake when neither of
 782 these scalings is correct.

783 While the effective uptake coefficients are our main focus in this paper, we have
 784 also determined effective diffusion coefficients for the upscaled problem. We briefly
 785 note that the important distinguished limit for the effective diffusion is given in Case
 786 1; the effective diffusion coefficient in Case 2 is a sublimit of Case 1 as the pointwise
 787 diffusion coefficient within the bacteria vanishes, and the effective diffusion coefficient
 788 in Case 3 is a sublimit of Case 1 as the bacterial radius vanishes.

789 With regards to the effective uptake, the general behaviour can be classified into
 790 two cases, depending on whether the typical bacterial radius is around the same
 791 size or much smaller than the distance between bacterial centres. When they are
 792 of the same order, the important distinguished limit occurs when the diffusion in
 793 the bacteria is small, in the double-porosity limit. This is Case 2, where there is a
 794 memory effect in the effective uptake, which is given as an explicit convolution of the
 795 nutrient concentration in terms of the system parameters in (38). Hence, the upscaling
 796 procedure converts a partial differential equation into an integro-differential equation.
 797 This memory effect can fade over time to produce a valid steady equation, providing

798 the external boundary conditions allow for this. In the steady case, the effective uptake
799 becomes an explicit linear function of the instantaneous nutrient concentration, and
800 we give an explicit result for the effective uptake coefficient σ in (40b). This explicit
801 result shows how the effective uptake smoothly varies between scaling with bacterial
802 volume and bacterial surface area, for a small and large reaction rate, respectively. In
803 this manner, the effective uptake in Case 1 can be derived as a sublimit of σ as the
804 pointwise diffusion coefficient within the bacteria becomes of the same order as the
805 diffusion coefficient within the passive medium.

806 When the typical bacterial radius is much smaller than the distance between
807 bacterial centres, the important distinguished limit occurs when the pointwise rate of
808 nutrient uptake is large. This is Case 3, where we derive an explicit analytic expression
809 for the effective uptake coefficient ν in (49). Notably, we find that ν is bounded above
810 as the pointwise rate of nutrient uptake increases, and the supremum of this scales
811 with the radii of the bacteria, as per the classic Smoluchowski result for uptake on
812 the surface of a single sphere. Since ν also scales with the volume of the bacteria for
813 a small pointwise uptake in this distinguished limit, we find that ν can scale from
814 anywhere between the radius to the volume of the bacteria. In this manner, the
815 effective uptake in Case 1 can be derived as a sublimit of ν as the pointwise uptake
816 within the bacteria grows very large and the bacterial radius becomes of the same
817 order as the distance between bacterial centres.

818 When mathematically modelling the nutrient uptake within a colony of growing
819 bacteria, one may derive and investigate a governing equation in terms of the bacterial
820 volume. In this paper, we have provided the correct uptake terms for such an equation
821 in terms of the bacterial properties. Even though we start from a linear pointwise
822 uptake, our work shows that the effective uptake should only scale linearly with the
823 bacterial volume under certain circumstances, notably when the pointwise uptake is
824 very weak. Otherwise, the effective uptake can scale with, for example, the bacterial
825 surface area or radius, and the uptake should thus be a nonlinear function of the
826 bacterial volume.

827 Although the main goal of this paper is to determine the effective uptake within
828 a colony of bacteria, by considering a negative uptake coefficient (corresponding to a
829 positive production coefficient) our results can be modified to investigate autocatalytic
830 production of some chemical or positive autoregulation of gene expression within
831 the bacteria. Our homogenized equations are still valid as the uptake coefficient
832 decreases through zero, but we show that the effective production rate will blow
833 up when the production coefficient reaches a critical value defined by (55) in Case
834 3. The corresponding result for Case 2 is a sublimit of the Case 3 result, when the
835 diffusion coefficient within the bacteria becomes much smaller than within the passive
836 medium. Since the dominant balance in the asymptotic scalings will change close to
837 this apparent blow up, it would be interesting to investigate the blow-up problem of
838 autocatalytic production in more detail.

839 As the leading-order concentration within the passive medium does not depend
840 on the microscale variable in all the cases we consider, we expect our effective uptake
841 results to hold for any Bravais lattice of spheres, with an appropriate scaling to account
842 for the relative volumes of the bacterial phase and the (locally) periodic cell. However,
843 the effective diffusion coefficients will not translate directly, as the geometry of the
844 cell problem will change. Our work in Case 1 can be applied directly to more general
845 arrays of spheres, and the relevant effective diffusion coefficients can be obtained from
846 (19c) by solving the cell problem (15) for different arrays. Additionally, in this paper
847 we have modelled the spatial variation in bacterial density by allowing the bacterial

848 radius to vary slowly in space. Another way to model this change in bacterial density
849 is to consider a slow variation in the lattice on which the bacterial centres lie. That is,
850 to consider a locally periodic lattice that varies slowly in space and use the methods
851 of [27] to transform this near-periodic microscale to a strictly periodic microscale. As
852 shown in [5], if we use a conformal transformation to preserve the spherical shape of
853 the bacteria, the nature of the Jacobian matrix of the transformation would result
854 in a greatly simplified cell problem for the diffusion coefficient. Moreover, as the
855 transformation only affects spatial derivatives, we would still expect our results for
856 the effective uptake to apply after the transformation. In this paper we have not
857 considered the problem of large pointwise uptake when the typical bacterial radius
858 is around the same size as the distance between bacterial centres. In such a case,
859 the uptake timescale would be much quicker than the timescale of diffusion over the
860 bioreactor lengthscale, yielding large depleted regions within the passive medium,
861 and the nutrient uptake would be localized to boundary layers near the bacterial
862 membrane.

863 We have used initial conditions that are continuous across the bacterial membrane
864 and allow for a slow variation in the concentration over the bioreactor lengthscale.
865 Although these initial conditions are idealized, the initial conditions of the system
866 are only significant in Case 2. Moreover, in Case 2 the effect of the initial conditions
867 decays over time. For more general initial conditions, we will have early-time boundary
868 layers where the initial conditions settle down. In Case 1, general initial conditions
869 will settle over a timescale of $t = O(\epsilon^2)$ to the conditions we use in this paper. In
870 Case 2, general initial conditions within the passive medium will become independent
871 of the short bacterial lengthscale over the same timescale, but the initial conditions
872 within the bacteria will only decay over a timescale of $t = O(1)$. In Case 3, general
873 initial conditions within the bacteria will settle to the steady state solution over a
874 timescale of $t = O(\epsilon^6)$, whereas general initial conditions within the passive medium
875 will settle over a timescale of $t = O(\epsilon^2)$.

876 In this paper we mainly consider bacteria with a spherical morphology, known
877 as *cocci*. Although this is a common morphology, there are other possible bacterial
878 shapes, ranging from the more prevalent rod-shaped (*bacilli*), to the more unusual
879 star-shaped (*stella*). In Appendix A we discuss the generalization of our results to
880 arbitrary bacterial shapes and we provide the systems that would have to be solved
881 to obtain the upscaled results for a given bacterial shape. Although explicit analytic
882 results are only possible in certain circumstances, the distinguished limits we discuss
883 in this paper provide the important scalings for arbitrary bacterial shapes under
884 the uptake form and coupling conditions we consider. Notably, in the limit of large
885 pointwise uptake in Case 3, we are able to obtain closed-form solutions for the effective
886 uptake by ellipsoidal bacteria in terms of the incomplete elliptic integral of the first
887 kind.

888 There are several further natural extensions to the work in this paper. For ex-
889 ample, we have neglected the role of advective transport in this model, allowing us
890 to focus on the three distinguished limits that arise with just diffusion and uptake as
891 the transport processes. The inclusion of advection would present more distinguished
892 limits in the system, and these could be explored by using the results in this paper as
893 a basis from which to extend. Another simplifying assumption we make is that the
894 uptake reaction has first-order kinetics. This results in a linear uptake term in the cell
895 problem, facilitating our analytic solutions to the cell problems and yielding explicit
896 terms for the effective uptake. This uptake term could be generalized to different
897 nonlinear reaction terms, such as Michaelis–Menten or Freundlich-type uptake terms,

898 and it may not be possible to obtain explicit analytic results for these cases.

899 We have neglected any internal structure of the bacteria, as we have assumed that
 900 the bacterial phases are homogeneous. Moreover, we have assumed a unit partition
 901 coefficient between the bacteria and the passive medium, as we took continuity of
 902 concentration through the bacterial membrane. It would be simple to modify the
 903 analytic results in this paper to account for a non-unit partition coefficient between
 904 the interior and exterior of the bacteria. If there were specific problems that required
 905 nonlinear coupling conditions or an inhomogeneous internal structure to be included,
 906 the framework we have developed in this paper could be extended to include such
 907 properties, but analytic results are unlikely. With recent advances in high-resolution
 908 imaging techniques for bacteria, such as those used in [13], one could develop a more
 909 accurate model of the bacterial interior, and use experimentally relevant bacterial
 910 shapes and distributions of bacteria, allowing the upscaling procedure to be performed
 911 on a more accurate description of the microstructure.

912 In this paper, we have investigated and quantified how the effective uptake scales
 913 with bacterial properties such as size, diffusivity, and pointwise uptake. We have
 914 shown when it is valid to scale the effective uptake with the bacterial volume, when
 915 scaling with the surface area is more appropriate, how to transition between these two
 916 scalings, and how to identify and deal with the case when neither scaling is correct.
 917 Moreover, the diffusion–reaction system we consider is not just limited to bacteria,
 918 and can also be applied to other single-celled microorganisms, such as cyanobacteria,
 919 microalgae, protozoa, and yeast. More generally, solute transport problems are near
 920 ubiquitous in applied mathematics, and the framework of this paper can be extended
 921 to consider other particular problems. We hope that our systematic upscaling results
 922 will be used to impose accurate effective uptake rates for general models of solute
 923 uptake in as wide a range of physical areas as possible.

924 **Acknowledgements.** This work was supported by the Biotechnology and Bio-
 925 logical Sciences Research Council [grant number BB/L013940/1]; and the Engineering
 926 and Physical Sciences Research Council, jointly funding the first grant number.

927 **Appendix A. General-shaped bacteria.**

928 In this Appendix, we consider some generalizations of our results to non-spherical
 929 bacteria, in part to emphasize the broader applicability of the above methodologies.
 930 For notational brevity, we still refer to the bacterial and medium domains as $\omega_b(\mathbf{x})$
 931 and $\omega_m(\mathbf{x})$, respectively. For Case 1, it is simple to deduce that (19a), the effective
 932 governing equation, becomes

$$933 \quad (A1) \quad \frac{\partial \hat{c}}{\partial t} = \nabla_{\mathbf{x}} \cdot (\mathbf{D}(\mathbf{x}) \nabla_{\mathbf{x}} \hat{c}) - \mu |_{\omega_b(\mathbf{x})} \hat{c},$$

935 where \mathbf{D} is a tensor equal to the right-hand side of (19c), requiring solutions to the
 936 cell problem (15) with arbitrary bacterial and medium domains.

937 For Case 2, the effective governing equations are still given by (34)–(35), but we
 938 note that it is difficult to give an analytic solution to (35) for a general-shaped bacterial
 939 domain. However, for a large pointwise uptake coefficient, $\hat{\mu} \gg 1$, the majority of the
 940 uptake is located in a boundary layer close to the bacterial membrane. To determine
 941 the concentration within this boundary layer, it is convenient to work in a general
 942 curvilinear coordinate system with n denoting the direction normal to the membrane
 943 such that $n = 0$ on the bacterial membrane, with $n > 0$ corresponding to the passive
 944 medium and $n < 0$ corresponding to the bacterial domain. Then, in the limit $\hat{\mu} \gg 1$,

945 the asymptotic solution to (35) is

$$946 \quad (A2) \quad C_0 \sim \widehat{c}(\mathbf{x}, t) e^{\hat{\mu}^{1/2} n}.$$

948 Using this result in (34), the effective governing equation for the intrinsic-averaged
949 concentration for general-shaped bacteria is

$$950 \quad (A3) \quad |\omega_m(\mathbf{x})| \frac{\partial \widehat{c}}{\partial t} = \nabla_{\mathbf{x}} \cdot (|\omega_m(\mathbf{x})| \overline{D}(\mathbf{x}) \nabla_{\mathbf{x}} \widehat{c}) - \hat{\mu}^{1/2} \hat{D} |\partial \omega_b(\mathbf{x})| \widehat{c}.$$

952 This result generalizes the large $\hat{\mu}$ result for *cocci* that we derived in (43b) for the
953 steady state, showing that the effective uptake coefficient is the product of the point-
954 wise uptake $\hat{\mu} \hat{D}$, the width of the boundary layer within a bacterium $\hat{\mu}^{-1/2}$, and the
955 surface area of the bacteria $|\partial \omega_b(\mathbf{x})|$. Noting that the volumetric-averaged concen-
956 tration $\bar{c} = |\omega_m(\mathbf{x})| \widehat{c} + O(\hat{\mu}^{-1/2})$ for large $\hat{\mu}$, we can also write the following effective
957 governing equation for the volumetric-averaged concentration with general-shaped
958 bacteria:

$$959 \quad (A4) \quad \frac{\partial \bar{c}}{\partial t} = \nabla_{\mathbf{x}} \cdot \left(\overline{D}(\mathbf{x}) \nabla_{\mathbf{x}} \bar{c} - \frac{\nabla_{\mathbf{x}} |\omega_m(\mathbf{x})|}{|\omega_m(\mathbf{x})|} \bar{c} \right) - \hat{\mu}^{1/2} \hat{D} \frac{|\partial \omega_b(\mathbf{x})|}{|\omega_m(\mathbf{x})|} \bar{c}.$$

961 Here, we note the appearance of an effective advection term which arises due to spatial
962 variation in bacterial volume, as expected for diffusion past impermeable obstacles [5].
963 Additionally, we note that the effective uptake in (A4) has an equivalent geometrical
964 dependence to the effective uptake in the simpler (single-phase) problem with partial
965 adsorption on the surface of obstacles arranged in a periodic array. This single-phase
966 case is considered in [10, 11] and is a similar but reduced version of the problem
967 considered in this paper, as the concentration evolution within the bacterial/obstacle
968 phase is not considered. To obtain the model in [10, 11], the dimensional governing
969 equation (2b) and interfacial conditions (2c,d) should be replaced with the dimensional
970 boundary condition

$$971 \quad (A5) \quad \mathbf{n} \cdot D_m \nabla \tilde{c} = -\gamma \tilde{c} \quad \text{for } \tilde{\mathbf{x}} \in \partial \Omega_b.$$

973 Comparing the effective uptake results for surface adsorption in [10, 11] with the
974 effective uptake for volume sinks with large pointwise coefficient in (A4), we deduce
975 that an equivalent effective uptake is obtained when $\gamma = (\lambda D_b)^{1/2}$, recalling that λ is
976 the dimensional volume uptake coefficient in this paper.

977 To generalize Case 3, we re-define the bacterial domain in the inner domain using
978 $\overline{\omega_b}(\mathbf{x})$ instead of $\omega_b(\mathbf{x})$, where $|\omega_b| = \epsilon^6 |\overline{\omega_b}|$ and $|\overline{\omega_b}| = O(1)$. For the spherical case
979 in §3.3, this volume scaling is implied by the radial scaling $R = \epsilon^2 \bar{R}$.

980 Then, using the scaling $\mathbf{y} = \epsilon^2 \mathbf{Y}$, the leading-order system (46) becomes

$$981 \quad (A6a) \quad \nabla_{\mathbf{Y}}^2 c = 0 \quad \text{for } \mathbf{Y} \in \mathbb{R}^3 \setminus \overline{\omega_b}(\mathbf{x}),$$

$$982 \quad (A6b) \quad \nabla_{\mathbf{Y}}^2 C - \bar{\mu} C = 0 \quad \text{for } \mathbf{Y} \in \overline{\omega_b}(\mathbf{x}),$$

$$983 \quad (A6c) \quad c = C \quad \text{for } \mathbf{Y} \in \partial \overline{\omega_b}(\mathbf{x}),$$

$$984 \quad (A6d) \quad \frac{\partial c}{\partial n} = D \frac{\partial C}{\partial n} \quad \text{for } \mathbf{Y} \in \partial \overline{\omega_b}(\mathbf{x}),$$

$$985 \quad (A6e) \quad c \rightarrow c_0(\mathbf{x}, t) \quad \text{as } |\mathbf{Y}| \rightarrow \infty.$$

987 The effective governing equation is then given by (51), using

$$988 \quad (A7) \quad \nu = \frac{1}{c_0(\mathbf{x}, t)} \int_{\partial \overline{\omega_b}(\mathbf{x})} \frac{\partial c}{\partial n} ds,$$

989

990 where ds denotes a surface element of the bacterial membrane and c is a solution to
 991 the coupled system (A6). As with the generalized Case 2, we are unable to solve (A6)
 992 analytically for a general-shaped bacterial domain. We are able to make further ana-
 993 lytic progress in the limit of large $\bar{\mu}$, when the problems in each phase decouple from
 994 one another. In this case, there is a boundary layer within each bacterium near the
 995 bacterial membrane, where the concentration decreases exponentially with argument
 996 $\sqrt{\bar{\mu}n}$, in a similar manner to (A2). However, the pre-factor of this exponential is not
 997 known *a priori*, and must be determined by solving the decoupled system for c , given
 998 by

$$999 \quad (\text{A8a}) \quad \nabla_{\mathbf{Y}}^2 c = 0 \quad \text{for } \mathbf{Y} \in \mathbb{R}^3 \setminus \bar{\omega}_b(\mathbf{x}),$$

$$1000 \quad (\text{A8b}) \quad c = 0 \quad \text{for } \mathbf{Y} \in \partial\bar{\omega}_b(\mathbf{x}),$$

$$1001 \quad (\text{A8c}) \quad c \rightarrow c_0(\mathbf{x}, t) \quad \text{as } |\mathbf{Y}| \rightarrow \infty.$$

1003 Thus, from (A7) we see that the effective uptake coefficient can be determined by
 1004 solving (A8) and, notably, we see that the effective uptake coefficient is independent
 1005 of $\bar{\mu}$ and D in the large $\bar{\mu}$ limit.

1006 We may obtain an analytic expression for the solution to (A8), and hence the
 1007 effective uptake coefficient, for ellipsoidal bacteria, exploiting the separability of the
 1008 Laplace operator in ellipsoidal coordinates.¹ For brevity, we consider a strictly pe-
 1009 riodic array of bacteria, define the longest semi-axis to have length \bar{R} , and scale
 1010 $\mathbf{Y} = \bar{R}\bar{\mathbf{Y}}$, such that the bacterial region in one periodic cell is defined as

$$1011 \quad (\text{A9}) \quad \bar{\omega}_b := \left\{ \bar{\mathbf{Y}} \in \mathbb{R}^3 : \bar{Y}_1^2 + \frac{\bar{Y}_2^2}{\alpha^2} + \frac{\bar{Y}_3^2}{\beta^2} < 1 \right\}.$$

1013 Here, \bar{Y}_i for $i = 1, 2, 3$ are three Cartesian components of $\bar{\mathbf{Y}}$. Without loss of gener-
 1014 ality, we are able to orient these axes to coincide with the semi-axes of the ellipsoidal
 1015 bacteria; on the lengthscale of the homogenization cell, the apparent point sink from
 1016 bacterial uptake has no preferred angle. Additionally, the two constants α and β sat-
 1017 isfy $0 < \beta \leq \alpha \leq 1$, again without loss of generality. Spherical bacteria are obtained
 1018 when $\alpha = \beta = 1$. By transforming to ellipsoidal coordinates, the solution to (A8) can
 1019 be written as

$$1020 \quad (\text{A10}) \quad c = c_0(\mathbf{x}, t) \left(1 - \frac{F\left(\frac{\sqrt{1-\beta^2}}{\zeta(\bar{\mathbf{Y}})}; \sqrt{\frac{1-\alpha^2}{1-\beta^2}}\right)}{F\left(\sqrt{1-\beta^2}; \sqrt{\frac{1-\alpha^2}{1-\beta^2}}\right)} \right),$$

1022 where

$$1023 \quad (\text{A11}) \quad F(x; k) = \int_0^x \frac{ds}{\sqrt{(1-s^2)(1-k^2s^2)}},$$

¹We note that a similar geometry in (A6) would also be analytically tractable, as the Helmholtz operator is also separable in ellipsoidal coordinates, but this is beyond the scope of this paper.

1025 is the incomplete elliptic integral of the first kind.² Here, $\zeta^2(\bar{\mathbf{Y}})$ is defined as the
 1026 solution to the following cubic in ζ^2 :

$$1027 \quad (A12) \quad \frac{\bar{Y}_1^2}{\zeta^2} + \frac{\bar{Y}_2^2}{\zeta^2 + \alpha^2 - 1} + \frac{\bar{Y}_3^2}{\zeta^2 + \beta^2 - 1} = 1,$$

1029 where $\zeta(\bar{\mathbf{Y}}) \geq 1$, with equality defining the ellipsoidal surface. Rather than directly
 1030 evaluating (A7) to determine the effective uptake, it is simpler to expand (A10) in the
 1031 large ζ limit, accounting for the scaling $\mathbf{Y} = \bar{R}\bar{\mathbf{Y}}$, then use the divergence theorem
 1032 to deduce that

$$1033 \quad (A13) \quad \nu = \frac{4\pi\bar{R}\sqrt{1-\beta^2}}{F\left(\sqrt{1-\beta^2}; \sqrt{\frac{1-\alpha^2}{1-\beta^2}}\right)}.$$

1034
 1035 We show how ν varies with α and β in figure 7. Of particular interest are the sub-
 1036 cases of oblate and prolate spheroids, being plausible geometries for some bacteria.
 1037 An oblate spheroid corresponds to $\alpha = 1$ with $\beta < 1$, resulting in an effective uptake

$$1038 \quad (A14) \quad \nu = \frac{4\pi\bar{R}\sqrt{1-\beta^2}}{\sin^{-1}\sqrt{1-\beta^2}}.$$

1040 A prolate spheroid corresponds to $\alpha = \beta < 1$, resulting in an effective uptake

$$1041 \quad (A15) \quad \nu = \frac{4\pi\bar{R}\sqrt{1-\beta^2}}{\tanh^{-1}\sqrt{1-\beta^2}}.$$

1043 As bacilli or coccobacilli can be modelled as prolate spheroids, (A15) gives the effective
 1044 uptake through either such colony in the limits of large pointwise uptake and large
 1045 separation between bacteria. Additionally, in the limit of $\beta \rightarrow 0$, we note that the
 1046 effective uptake is finite for $\alpha > 0$ (where the bacteria is a two-dimensional disk),
 1047 but vanishes with a logarithmic dependence when we also consider $\alpha \rightarrow 0$ (where the
 1048 bacteria is a one-dimensional rod). Thus, long thin bacteria with a large separation
 1049 distance will have a negligible effect on removing nutrient from the system, even when
 1050 their pointwise uptake is very large. We also note that in the special case of spherical
 1051 bacteria, attained in the limits $\alpha \rightarrow 1$ and $\beta \rightarrow 1$, the effective uptake reduces to that
 1052 of (54), as expected.

1053 REFERENCES

- 1054 [1] T. ARBOGAST, J. DOUGLAS, JR, AND U. HORNUNG, *Derivation of the double porosity model of*
 1055 *single phase flow via homogenization theory*, SIAM J Math. Anal., 21 (1990), pp. 823–836.
 1056 [2] A. G. BELYAEV, A. L. PYATNITSKII, AND G. A. CHECHKIN, *Asymptotic behavior of a solution*
 1057 *to a boundary value problem in a perforated domain with oscillating boundary*, Siberian
 1058 Math. J., 39 (1998), pp. 621–644.
 1059 [3] A. BENSOUSSAN, J.-L. LIONS, AND G. PAPANICOLAOU, *Asymptotic analysis for periodic struc-*
 1060 *tures*, North-Holland Publishing Company, Amsterdam, 1978.
 1061 [4] R. B. BIRD, W. E. STEWART, AND E. N. LIGHTFOOT, *Transport phenomena*, John Wiley &
 1062 Sons, 2007.

²We give (A11) in Jacobi’s form here for notational purposes, though we note that the trigono-
 metric form is more amenable to numerical calculation when $\beta \rightarrow 0$ and thus when $x \rightarrow 1$ in (A11).

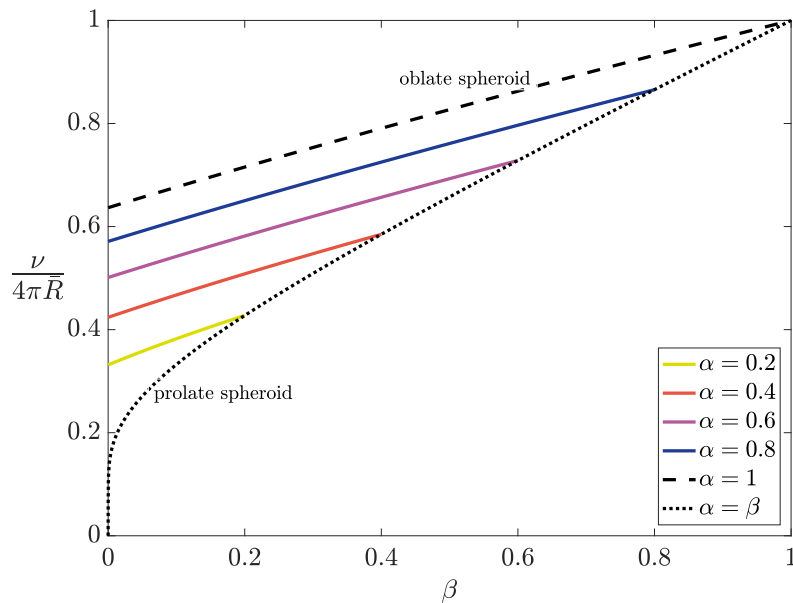


FIG. 7. The normalized effective uptake, $\nu/(4\pi\bar{R})$, for small ellipsoidal bacteria in the limit of large uptake, as given in (A13). The principal semi-axes have lengths \bar{R} , $\alpha\bar{R}$, and $\beta\bar{R}$, where $0 < \beta \leq \alpha \leq 1$. The case where $\alpha = 1$ corresponds to an oblate spheroid, and the case where $\alpha = \beta$ corresponds to a prolate spheroid.

- 1063 [5] M. BRUNA AND S. J. CHAPMAN, *Diffusion in spatially varying porous media*, SIAM J. Appl.
 1064 Math., 75 (2015), pp. 1648–1674.
 1065 [6] S. J. CHAPMAN, D. P. HEWETT, AND L. N. TREFETHEN, *Mathematics of the Faraday cage*,
 1066 SIAM Review, 57 (2015), pp. 398–417.
 1067 [7] G. A. CHECHKIN AND A. L. PIATNITSKI, *Homogenization of boundary-value problem in a locally*
 1068 *periodic perforated domain*, Appl. Anal., 71 (1998), pp. 215–235.
 1069 [8] D. CIORANESCU AND F. MURAT, *A strange term coming from nowhere*, in Topics in the math-
 1070 *ematical modelling of composite materials*, Springer, 1997, pp. 45–93.
 1071 [9] C. CONCA, A. LIÑÁN, AND C. TIMOFTE, *Homogenization in chemical reactive flows*, Electron.
 1072 J. Differ. Equations, 40 (2004), pp. 1–22.
 1073 [10] M. P. DALWADI, M. BRUNA, AND I. M. GRIFFITHS, *A multiscale method to calculate filter*
 1074 *blockage*, J. Fluid Mech., 809 (2016), pp. 264–289.
 1075 [11] M. P. DALWADI, I. M. GRIFFITHS, AND M. BRUNA, *Understanding how porosity gradients can*
 1076 *make a better filter using homogenization theory*, Proc. R. Soc. A, 471 (2015).
 1077 [12] Y. DAVIT, C. G. BELL, H. M. BYRNE, L. A. C. CHAPMAN, L. S. KIMPTON, G. E. LANG, K. H. L.
 1078 LEONARD, J. M. OLIVER, N. C. PEARSON, R. J. SHIPLEY, S. L. WATERS, J. P. WHITELEY,
 1079 B. D. WOOD, AND M. QUINTARD, *Homogenization via formal multiscale asymptotics and*
 1080 *volume averaging: How do the two techniques compare?*, Adv. Water Resour., 62 (2013),
 1081 pp. 178–206.
 1082 [13] K. DRESCHER, J. DUNKEL, C. D. NADELL, S. VAN TEEFFELLEN, I. GRNJA, N. S. WINGREEN,
 1083 H. A. STONE, AND B. L. BASSLER, *Architectural transitions in Vibrio cholerae biofilms at*
 1084 *single-cell resolution*, Proc. Natl. Acad. Sci. USA, 113 (2016), pp. E2066–E2072.
 1085 [14] T. FATIMA, N. ARAB, E. P. ZEMSKOV, AND A. MUNTEAN, *Homogenization of a reaction-*
 1086 *diffusion system modeling sulfate corrosion of concrete in locally periodic perforated do-*
 1087 *mainis*, J. Eng. Math., 69 (2011), pp. 261–276.
 1088 [15] M. GAHN, M. NEUSS-RADU, AND P. KNABNER, *Homogenization of reaction-diffusion processes*
 1089 *in a two-component porous medium with nonlinear flux conditions at the interface*, SIAM
 1090 J. Appl. Math., 76 (2016), pp. 1819–1843.
 1091 [16] M. H. HOLMES, *Introduction to Perturbation Methods*, vol. 20, Springer Science & Business
 1092 Media, 2012.
 1093 [17] U. HORNUNG, *Homogenization and porous media*, vol. 6, Springer Science & Business Media,

- 1094 2012.
- 1095 [18] U. HORNUNG, W. JÄGER, AND A. MIKELIĆ, *Reactive transport through an array of cells with*
1096 *semi-permeable membranes*, Math. Model. Numer. Anal., 28 (1994), pp. 59–94.
- 1097 [19] V. V. JIKOV, S. M. KOZLOV, AND O. A. OLEINIK, *Homogenization of differential operators and*
1098 *integral functionals*, Springer Science & Business Media, 2012.
- 1099 [20] J. D. KEASLING, *Manufacturing molecules through metabolic engineering*, Science, 330 (2010),
1100 pp. 1355–1358.
- 1101 [21] P. A. LEVIN AND E. R. ANGERT, *Small but mighty: cell size and bacteria*, Cold Spring Harbor
1102 Perspec Biol, 7 (2015), p. a019216.
- 1103 [22] H. MÁRKL, C. ZENNECK, A. C. H. DUBACH, AND J. C. OGBONNA, *Cultivation of escherichia coli*
1104 *to high cell densities in a dialysis reactor*, Appl Microbiol Biotech, 39 (1993), pp. 48–52.
- 1105 [23] F. MURAT AND D. CIORANESCU, *Un terme étrange venu d'ailleurs*, in Non-Linear Partial Dif-
1106 ferential Equations and Their Applications, Volumes II and III, Collège de France Seminar,
1107 1982, pp. 98–138.
- 1108 [24] M. PANFILOV, *Macroscale models of flow through highly heterogeneous porous media*, vol. 16,
1109 Springer Science & Business Media, 2013.
- 1110 [25] M. PTASHNYK, T. ROOSE, AND G. J. D. KIRK, *Diffusion of strongly sorbed solutes in soil: a*
1111 *dual-porosity model allowing for slow access to sorption sites and time-dependent sorption*
1112 *reactions*, Eur. J. Soil Sci., 61 (2010), pp. 108–119.
- 1113 [26] N. RAY, T. ELBINGER, AND P. KNABNER, *Upscaling the flow and transport in an evolving porous*
1114 *medium with general interaction potentials*, SIAM J. Appl. Math., 75 (2015), pp. 2170–
1115 2192.
- 1116 [27] G. RICHARDSON AND S. J. CHAPMAN, *Derivation of the bidomain equations for a beating heart*
1117 *with a general microstructure*, SIAM J. Appl. Math., 71 (2011), pp. 657–675.
- 1118 [28] E. SÁNCHEZ-PALENCIA, *Non-homogeneous media and vibration theory*, in Lecture Notes in
1119 Physics, vol. 127, Springer-Verlag, Berlin, 1980.
- 1120 [29] R. J. SHIPLEY AND S. J. CHAPMAN, *Multiscale modelling of fluid and drug transport in vascular*
1121 *tumours*, B. Math. Biol., 72 (2010), pp. 1464–1491.
- 1122 [30] M. VAN DYKE, *Perturbation methods in fluid dynamics*, Parabolic Press, 1975.
- 1123 [31] T. L. VAN NOORDEN, *Crystal precipitation and dissolution in a porous medium: effective equa-*
1124 *tions and numerical experiments*, Multiscale Model. Simul., 7 (2009), pp. 1220–1236.
- 1125 [32] T. L. VAN NOORDEN AND A. MUNTEAN, *Homogenisation of a locally periodic medium with*
1126 *areas of low and high diffusivity*, Eur. J. Appl. Math., 22 (2011), pp. 493–516.
- 1127 [33] S. WHITAKER, *The method of volume averaging*, vol. 13, Springer Science & Business Media,
1128 2013.